Available online at www.sciencedirect.com
SCIENCE DIRECT
Polymer 46 (2005) 7874–7895
polymer
www.elsevier.com/locate/polymer

Radical entry mechanisms in redox-initiated emulsion polymerizations

David J. Lamb, Christopher M. Fellows[1], Robert G. Gilbert*

School of Chemistry F11, Key Center for Polymer Colloids, The University of Sydney, NSW 2006, Australia

Received 25 February 2005; received in revised form 21 June 2005; accepted 21 June 2005
Available online 19 July 2005

Abstract

The mechanisms and kinetics of radical entry in emulsion polymerizations utilizing redox initiation are investigated using polymerization rate data obtained by reaction calorimetry and electrospray mass spectroscopy analysis of initiator-derived aqueous-phase products. These data have been used to evaluate an initiation scheme for redox-initiated emulsion polymerizations of common monomers such as styrene and methyl methacrylate based around the oxidant, *tert*-butyl hydroperoxide. Redox initiators are broadly classed by the solubility of their radical products: Hydrophilic radicals enter by propagating to a critical degree of polymerization to become surface-active whilst more hydrophobic radicals may enter particles directly. When direct entry is applicable (the hydrophobic case), initiation efficiency will always be very high.

Keywords: Emulsion polymerization; Redox; Free radical

1. Introduction

Redox initiators are used extensively for emulsion polymerization of vinylic compounds. Radicals can be produced very rapidly compared to thermal initiators such as persulfate, and with reduced temperature constraints. Industrially, redox initiation has widespread application in monomer removal at the end of reaction ('chasing') and to the production of polymers at low temperatures, such as styrene/butadiene. Despite this technical importance, these systems have not seen the same level of mechanistic and kinetic study as those utilizing thermal initiators.

The key mechanistic differences between the thermal and redox initiation of emulsion polymerizations are in the entry step(s), whereby radical species are transferred from the aqueous phase, where they are generated, to the locus of polymerization, i.e. the particle phase. There is extensive evidence [1–5] that radical entry in conventional, thermally-initiated, electrostatically stabilized emulsion polymerizations is well described by the so-called 'Maxwell–Morrison' model [6]. This describes entry as arising from hydrophilic radicals $I^{\cdot}$ formed in the water phase from initiator decomposition (e.g. $SO_4^{-\cdot}$ produced from persulfate ions, $S_2O_8^{2-}$) that must propagate with the monomer (M) present in the aqueous phase (in low concentrations) to form the species $^{\cdot}M_zI$ (where z is the critical degree of polymerization for entry). These species are sufficiently surface-active to adsorb onto the surface of latex particles for enough time so that the radical end irreversibly enters the interior of the particle phase by further propagation. These events compete with aqueous-phase termination, which may lead to entry efficiencies significantly less than 100%. The reduction of initiator efficiency has a strong dependence on z and on aqueous phase monomer concentration, and so at high initiator concentrations it is common to observe low (i.e. 10% or lower) efficiencies.

A limiting form of this entry model is a system that results in the production of hydrophobic radicals from initiator in the water phase; sufficiently hydrophobic radicals will not require aqueous-phase propagation prior to entry, i.e. $z=1$. This removes the susceptibility to aqueous-phase termination, and hence entry efficiencies close to 100% may be achieved. The use of redox initiation systems may result in hydrophilic and/or hydrophobic radicals and so both limits of high and low efficiency may be present (even simultaneously). The motivation of this work is to explore a categorization for common redox initiation systems based upon radical solubility and the

* Corresponding author. Tel.: +61 2 9351 3366; fax: +61 2 9351 8651.
E-mail address: gilbert@chem.usyd.edu.au (R.G. Gilbert).
[1] Present address: School of Biological, Biomedical, and Molecular Sciences, University of New England, Armidale, NSW 2351, Australia.

0032-3861/$ - see front matter © 2005 Elsevier Ltd. All rights reserved.
doi:10.1016/j.polymer.2005.06.078

related initiator efficiency. For this purpose, it is essential to establish conditions whereby reproducible polymerization rates may be obtained using redox initiation. As is known within industry, and explored here, redox systems are very susceptible to the presence of trace (catalytic) amounts of transition-metal ions, or 'accelerants', and this will also be addressed in this study.

The key aspects of the initiation and entry kinetics with such systems will be described in terms of the hydrophilicity of the radical species produced. This requires means to measure the entry efficiency (or rate coefficient) in a redox system. Now, the methodologies which have been developed to obtain entry rate coefficients in emulsion polymerizations involve accurate determination of reaction rates, including under non-steady-state conditions [7]. Gravimetric determination of rates cannot produce data of sufficient accuracy for this purpose, and dilatometry has usually been employed to obtain rate data of sufficient precision. However, accurate dilatometry is very hard to implement under the feed conditions that are typical for redox systems, and hence the means of choice for obtaining rate data in the present study is calorimetry [8–16].

It is frequently assumed that the rate coefficient for radical production by the oxidizing and reducing components of a redox couple is high, resulting in a radical flux that is much higher than for typical thermal initiation conditions (for this reason, it is common to feed in one or both components of a redox initiation during the course of a reaction). If indeed the rate coefficient for radical production between the two moieties of a redox couple is extremely large, then there is the possibility of carrying out studies of radical loss rates by switching off the initiator feed and observing the decrease in rate, analogous to the 'γ-radiolysis relaxation' method which has led to considerable insight into radical loss processes in a range of emulsion polymerization systems [5,17,18]. If the reaction rate between the components of the redox couple is sufficiently high, then radical flux would cease virtually immediately after feed has been switched off in a redox system. The resulting change in rate would then yield reliable data for the rate coefficient for exit, and hence entry efficiency [5]. However, hints have emerged [19] that, at least for some redox couples such as cumyl hydropreroxide and tetraethylene pentamine, this redox rate coefficient may not be fast enough to be considered non-rate-determining. In the present paper, elucidation of this point will be sought from observed rate data after feed has been switched off, in addition to an exploration of the dynamic response limits of reaction calorimetry.

The monomers studied were styrene and methyl methacrylate (MMA), and the redox systems were be *tert*-butyl hydroperoxide (TBHP) with a variety of reductants: Sodium formaldehyde sulfoxylate (SFS), sodium metabisulfite (SMB) and ascorbic acid (ASA). The structures of these species are given in Fig. 1.

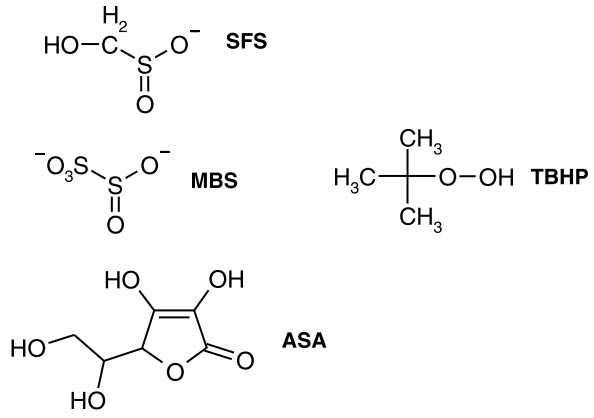

Fig. 1. Chemical structure of the oxidant, *tert*-butyl hydroperoxide (TBHP), and reductants, sodium formaldehyde sulfoxylate (SFS), sodium metabisulfite (MBS) (both only shown as anions) and ascorbic acid (ASA), used in this study.

2. Strategy

2.1. Entry mechanism

In order to understand the kinetics and mechanism of the redox systems used in this study the following approach is employed.

First, once the conditions for reproducible emulsion polymerizations of styrene and MMA have been established, the radical products formed in the water phase are examined by electrospray mass spectrometry (ES/MS). The end-groups of the water-soluble oligomers formed under redox initiation provide evidence for the initiation mechanisms of these redox systems. The reduction of TBHP to a *tert*-butoxy radical and a hydroxyl ion must involve the formation of a second radical species, for the case of the single redox reaction of TBHP with another species such as SFS. This compares to, for example, ASA, which can be doubly oxidized into a non-radical species that would have a different reactivity to the single oxidized radical. It is thus reasonable to expect that these species also play a key role in shaping the kinetics and physical properties of these emulsion polymerizations and it should be noted that this is an aspect that is not often considered.

Second, the kinetics of redox-initiated, seeded, styrene emulsion polymerizations are studied (by reaction calorimetry) to develop understanding of the kinetics of radical production and entry. Styrene is used for kinetic studies (rather than MMA) due to the large quantity of such work that has been previously published for thermally initiated, seeded emulsion polymerizations, and, therefore, any new aspects of the kinetics in this work are derived only from the redox initiation processes. Using the mechanisms that are consistent with the ES/MS data, polymerization rate data allow the overall rate of reaction under steady-state conditions to be equated to an entry rate. It is hypothesized that this entry rate is sufficiently different for hydrophobic radical species arising from hydrophilic initiating species

that initiation systems can be categorized upon the basis of primary radical solubility.

2.2. Zero-one/pseudo-bulk character

A convenient categorization of emulsion polymerization kinetics is into systems which are either 'zero-one' or 'pseudo-bulk' [7,20,21]. Zero-one systems are those in which entry of a radical into a particle which already contains a growing chain results in very rapid termination; in this case, intra-particle termination is not rate-determining, and the steady-state value of the average number of radicals per particle, $\bar{n}$, cannot exceed 1/2. In a pseudo-bulk system, radicals move frequently between particles and/or $\bar{n}$ is large, and thus the rate-determining events include intra-particle termination; these systems are kinetically equivalent to a bulk system (note that in a pseudo-bulk system, $\bar{n}$ can take any value, including less than 1/2).

These categorizations are particularly convenient for analyzing emulsion polymerization rate and molecular weight data with a minimum of model-based assumptions. Kinetic analysis of the 'no-man's land' between the two categories is complex [22] due to the dependence of the termination rate coefficient on the chain lengths of the terminating radicals, although means of treating experimental data while retaining some of the simplicity of the zero-one/pseudo-bulk dichotomy are starting to emerge [23].

While many emulsion polymerization systems fall conveniently into either one or the other category, it should be possible for a system to traverse from one to the other: For example, being zero-one with low radical flux, and moving to pseudo-bulk for higher radical flux. Redox initiation allows one to have a wide variation in radical flux, including being able to achieve fluxes higher than is the norm with thermal initiators. It, therefore, may be possible to traverse the gamut of behavior from zero-one to pseudo-bulk, by choosing a system which follows zero-one kinetics with thermal initiator and observing the dependence of the steady-state value of $\bar{n}$ with increasing radical flux using redox initiation, by increasing the redox feed rate. The system chosen for this purpose is a styrene system at 50 °C with particles in the size range established by Hawkett et al. [20] to obey zero-one kinetics with persulfate as initiator; this system is expected [7,24,25] to move out of zero-one kinetics once entry rates are extended beyond those possible with persulfate at this temperature. As this system is very well studied kinetically, with well-established values of the entry rate coefficient [5,26], this will provide a useful check on the methodology used in the present paper for inferring rate data in redox systems from reaction calorimetry.

2.3. Non-steady state kinetics and calorimetry

Non-steady state polymerization rate data (i.e. the 'relaxation' rate after the initiator feed is switched off) are also studied to ascertain kinetic information for the redox process itself, allowing estimates for the redox rate coefficients to be made based upon the calorimetric data. This not only can provide a way to determine such quantities but these studies have been used to explore the use of calorimetry for such dynamic determinations and asses the usefulness of the technique.

3. Experimental

3.1. Materials

All chemicals used in this study (*tert*-butyl hydroperoxide (TBHP, Aldrich), sodium formaldehyde sulfoxylate (SFS, Fluka), sodium metabisulfite (MBS, Sigma-Aldrich), ascorbic acid (ASA, Sigma-Aldrich), sodium persulfate (NaPS, Fluka), potassium persulfate (KPS, Sigma-Aldrich), Styrene (Synthetic Resins), methyl methacrylate (MMA, Sigma-Aldrich), iron sulfate, ($FeSO_4 \cdot 7H_2O$, Fluka), sodium hydrogencarbonate ($NaHCO_3$, Sigma-Aldrich), sodium dodecylsulfate (SDS, Sigma-Aldrich), Aerosol MA-80 (AMA-80, Cytec)) were used as supplied, with the exception of the two monomers which were passed through basic alumina prior to use for inhibitor removal. MilliQ water was used throughout this study.

3.2. Reaction calorimetry

The polymerizations reported in this study were performed in a Mettler-Toledo RC1*e* reaction calorimeter. The experimental details of such a system and the conversion of heat-flow data into polymerization rate have been described elsewhere [11,13,16,27]; it will suffice to mention that a HP-60 stainless steel reaction vessel was used with an anchor stirrer, and data were collected using the software package for Windows NT™ provided by the manufacturer. The polymerization rate R_p, and the corresponding value of $\bar{n}$, were obtained using:

$$R_p = \frac{\dot{Q}}{\Delta_{pol}H} \tag{1}$$

$$R_p = -\frac{d[\text{monomer}]_{react}}{dt} = k_p C_p \bar{n} \frac{N_p}{N_A} \tag{2}$$

where $\dot{Q}$ is the heat flow, $\Delta_{pol}H$ the enthalpy of polymerization of styrene, $[\text{monomer}]_{react}$ is the overall concentration of monomer in the reactor, k_p is the propagation rate coefficient, C_p is the monomer concentration inside the particles, N_p the particle number density, and N_A is the Avogadro constant. The value of k_p for this system was taken as $2.4 \times 10^2\ M^{-1}\ s^{-1}$ [28], $C_p = 5.5$ M [20] and $\Delta_{pol}H = 70\ kJ\ mol^{-1}$ [8,16].

3.3. Seed latex preparation

Polystyrene seed latexes were prepared for use in subsequent seeded experiments using the conditions given in Table 1. These latexes were produced in the RC1 reaction calorimeter and had average diameters of 31, 57, 103 and 127 nm as determined by dynamic light scattering (DLS—obtained with a Brookhaven BI-9000 instrument using an argon ion laser). TEM showed that the smallest latex was highly polydisperse, and its average size was obtained using DLS. Experiment [5,20] and theory [24,25,29] indicate that the three lowest sizes follow zero-one kinetics with persulfate initiator up to the maximum achievable concentration at 50 °C.

3.4. Seeded polymerizations of styrene

The first series of seeded polymerizations with redox initiation were performed using the 31 nm polystyrene latex to determine conditions under which the redox initiation systems were working reliably and reproducibly. In preliminary work performed using TBHP and SFS without the presence of an added metal catalyst (Fe^{2+}), low and irreproducible polymerization rates were observed for a variety of experimental conditions. A set of polymerizations, where the initiator solutions were fed into the reactor over a period of 2 h, were performed using the conditions outlined in Table 2, including the addition of a controlled amount of Fe^{2+} and a reduced pH, with greater success.

A series of seeded polymerizations was then performed using the 127 nm polystyrene latex to examine the effect of feed rate and reductant variation upon the polymerization kinetics with the reaction conditions given in Table 3. The feed concentrations given in the table are for the most concentrated feed, with dilutions by factors of 2 and 10 also used. The amount of SFS used is shown in the table (the equivalent amounts of MBS and ASA used in parallel studies were, 4.03 and 3.75 g, respectively). These initiator solutions were fed into the reactor at a feed rate of 1 g min^{-1}.

Table 1
Reaction conditions for the preparation of 31.0, 57.2, 103 and 127 nm polystyrene seed latexes used throughout this study

Component/condition	31.0 nm	57.2 nm	103 nm	127 nm
Styrene (g)	75.0	250	250	300
Water (g)	1300	733	825	600
SDS (g)	9.75	5.0		–
AMA-80 (g)	–	–	15.0	10.5
$NaHCO_3$ (g)	1.5	0.5	1.25	1.0
KPS (g)	3.00 (in 30 g H_2O)	–	1.25 (in 50.0 g H_2O)	1.0 (in 30 g H_2O)
NaPS (g)	–	2.5 (in 10 g H_2O)		–
Reaction temperature (°C)	90	90	90	90
Vessel type	Stainless steel	Stainless steel	Stainless steel	Stainless steel
Agitation (rpm)	300	300	300	300

Table 2
Reaction conditions for the seeded emulsion polymerization of styrene with the 31 nm seed latex using the TBHP and SFS initiation system to test redox reproducibility

Seed latex (g)/final dilution (g)	25/1000
Styrene (g) (charge/feed)	100
TBHP (g) (in 30 g H_2O)	1.91
SFS (g) (in 30 g H_2O)	3.27
$FeSO_4 \cdot 7H_2O$ (g) (in 30 g H_2O)[a]	0.014
Reaction temperature (°C)	50
Vessel type	Stainless steel
Agitation	250 rpm

[a] This solution was acidified with a few drops of concentrated HCl (latex pH = 2).

Further seeded styrene polymerizations were performed using the conditions outlined in Table 3 for both the 57.2 and 127 nm seed latexes. For all experiments the pumping rate was 1 g min^{-1} with a pumping period of 10 min and a relaxation period of 20 min. The initiator concentrations given in the table were the highest used; lower concentrations were also employed in various runs. Two experiments were performed with the 127 nm seed: With feed rates of 3.5×10^{-6} and 3.5×10^{-7} M s^{-1}, respectively. For experiments with the 57.2 nm seed latex, three concentrations were used: That given in Table 3 and with feed rates of 3.5×10^{-6}, 7.0×10^{-7} and 7.0×10^{-8} M s^{-1}.

The seeded experiments using the 103 nm latex with conditions given in Table 4 were performed to see if the system could traverse the range from zero-one to pseudo-bulk kinetics with increasing redox feed rate. In both cases materials were used as supplied, except that styrene monomer was passed through a basic alumina column prior to use. The seeded experiments had a particle number of 5.0×10^{16} dm^{-3}. The initiator was fed into the reactor as two feed lines: One feed of TBHP solution and the other of SFS solution. The concentrations of these two feeds were identical and the rage of concentrations across experiments, as percentages by weight, is given in Table 5. The feed conditions were kept at 1 g min^{-1} for each feed in all experiments.

Table 3
Reaction conditions for 'pulsed' seeded styrene emulsion polymerizations of styrene using both the 57.2 and 127 nm seed latex (for polymerizations using MBS and ASA molarity was kept equal to that indicated for SFS)

Seed (g)/final diluted mass (g)	200/1000
Styrene (g)	100
TBHP (g)	1.91 in 100 g H_2O
SFS (g)	3.27 in 100 g H_2O
$FeSO_4 \cdot 7H_2O$ (g)	0.014
Reaction temperature (°C)	50
Vessel type/agitation	Stainless steel/300 rpm

Table 4
Preparation of seeded polystyrene emulsion polymerization for testing the zero-one/pseudo-bulk traverse with increasing initiator feed rate

Seed latex/final dilution (g)	100/800
Styrene (g)	36.8
$FeSO_4 \cdot 7H_2O$ (g)	0.014
Reaction temperature (°C)	50
Vessel type/agitation	Stainless steel/200 rpm

Table 5
Feed conditions for the seeded styrene emulsion polymerizations of 103 nm seed with varying feed rates of TBHP (or other species) as weight percentages of feed solution

Feed concentration (%)	ρ (s^{-1})
0.1	2.8
1×10^{-2}	0.28
4×10^{-3}	1.1×10^{-1}
2×10^{-3}	5.7×10^{-2}
1×10^{-3}	2.8×10^{-2}

Also shown is the calculated value for ρ assuming diffusion-limited entry (Eq. (11)).

3.5. Molecular weight analysis

For some of the seeded polymerizations, a determination of the final molecular weight distribution was performed by size exclusion chromatography, SEC. The apparatus for these measurements was a Shimadzu/Waters SEC with UV and RI detection. Polystyrene standards were used for calibration spanning the range of molecular weights found in these experiments.

3.6. Ab initio polymerizations of methyl methacrylate

Ab initio surfactant-free emulsion polymerizations of MMA were performed in the RC1 reaction calorimeter, using TBHP/Fe with SFS, MBS or ASA as initiators. MMA was used as it is much more water-soluble than styrene (whose water solubility is $C_W^{sat} = 4.3\times10^{-3}$ M at 50 °C [30], compared to 6.1×10^{-1} M for MMA at the same temperature [31]), and thus will yield higher concentrations of water-phase species involved in the entry mechanism. These higher concentrations will be more readily detected. Preliminary work employing styrene was unable to produce any ES/MS spectra with a sufficient signal-to-noise ratio to identify water-soluble oligomeric species.

The experimental conditions are given in Table 6 and the resultant latexes or dispersions (these systems had no added surfactant) were centrifuged to obtain the aqueous phase for electrospray mass spectrometry (ES) analysis. The ES instrument was a Finnigan LCQ MS detector, utilizing both positive and negative ion detection, and the centrifugation was performed in a Beckman-Coulter Optima L-100 Ultracentrifuge (2×10^4 rpm for 30 min).

Table 6
Experimental conditions for ab initio, surfactant-free polymerizations of MMA by redox initiation using TBHP/Fe and indicated reductants

Conditions	SFS	ASA	MBS
MMA (g)	50.0	50.0	50.0
Water (g)	600	600	600
$FeSO_4 \cdot 7H_2O$ (g)	0.0172	0.0172	0.0172
TBHP (g) (in 30 g H_2O)[a]	2.36	1.87	5.0
SFS (g) (in 30 g H_2O)[a]	2.45	–	–
ASA (g) (in 30 g H_2O)[a]	–	2.5	–
MBS (g) (in 30 g H_2O)[a]	–	–	5.0
Reaction temperature (°C)	50	50	50
Vessel type	Stainless steel	Stainless steel	Stainless steel
Agitation (rpm)	200	200	200

[a] Initiator solutions were fed into the reactor at a rate of 1 g min^{-1}.

4. Results: Calorimetry and kinetics

4.1. Effect of metal catalyst on polymerization rate

As mentioned in the previous section, seeded emulsion polymerization of styrene performed using TBHP and SFS without addition of Fe^{2+} showed irregular and irreproducible polymerization rates and conversions. Fig. 2 shows the duplicate runs for such a polymerization but in the presence of a metal catalyst, Fe^{2+}, under acidic conditions. Under these experimental conditions, the initiation is clearly fast enough to generate pseudo-steady-state conditions, and so the polymerization rate can be assumed to be under the control of the entry rate and hence, the feed rate (see subsequent discussions on entry kinetics). The polymerization kinetics are clearly reproducible and these results show that for TBHP and SFS, the presence such a transition metal catalyst is crucial to generate reproducible polymerization conditions.

The uses of metal 'catalysts' are reported extensively in the patent literature for industrial processes [32–37], but it has sometimes been reported that these redox systems have been used without a metal catalyst (e.g. using similar redox protocols for ASA [38]). The necessity for iron was thoroughly tested specifically for TBHP/SFS in the present study, and the protocols developed were adopted for all other reductants. For example, it has been assumed here that, as the reactions of both TBHP and ASA acid with iron are well known, a catalytic reaction pathway will be followed. If this is not the case and a different direct pathway occurs between TBHP and ASA, then it is unlikely to be affected by the trace amounts of iron present.

4.2. Effect of reductant on polymerization rate

Data are presented in Fig. 3 for the polymerization rate of

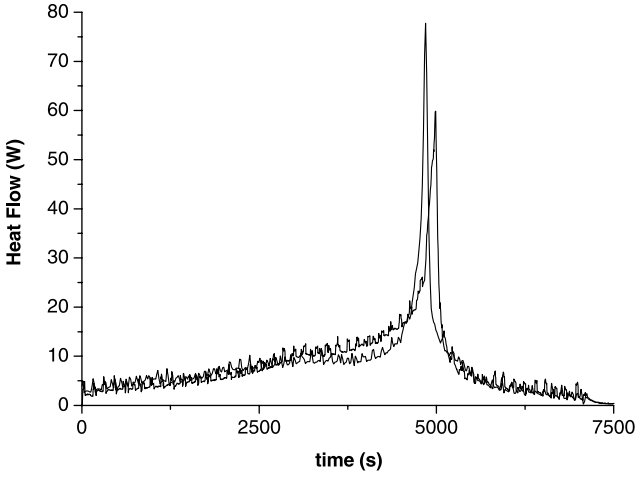

Fig. 2. Duplicate seeded styrene emulsion polymerization rate data, as reaction heat flows, using the TBHP/Fe/SFS redox initiation system (experimental conditions in Table 2) demonstrating system reproducibility.

seeded styrene emulsion polymerizations initiated by TBHP with ASA, SFS and MBS for the three different feed rates given in the previous section. These results show that rates of polymerization observed for the SFS and ASA systems with the overall rate increasing with initiator concentration and steady-state polymerization rates resulting from steady feed conditions. MBS, however, showed rates that were poorly controlled by the feed rate, i.e. clean steady-state rates were not observed and the polymerization rate did not appear to increase with the initiator feed concentration. The lack of control by feed with MBS may be due to the reaction conditions being sub-optimal, or to another effect, but it was deemed that this system was not suitable for further kinetic study, although the reaction products were still examined.

Another observation is that it is seen that the polymerization rate does not fall to zero in all cases, even some time after the cessation of initiator feed; this 'spontaneous' or 'background' polymerization is well known in emulsion systems [17,20,39–42]. The steady-state and post-feed heat flows are given in Table 7.

4.3. Emulsion polymerization kinetics and redox initiation

Seeded emulsion polymerizations of styrene using TBHP and SFS were performed using the 57.2 and 127 nm styrene latexes for kinetic analysis of their rate of approach to steady state, steady state and 'relaxation' (i.e. when the initiator feed is stopped). These data are shown in Fig. 4, where the initiator 'pulse' for the two 127 nm seed polymerizations leads to steady-state $\bar{n}$ values of 1.29 and 1.03 for the two feed conditions and the initiator pulse for the 57 nm seed yielded values for $\bar{n}$ of 0.75, 0.55, and 0.37. Observations were also able to be made for the 'spontaneous' $\bar{n}$. For the 127 nm seed latex the observed $\bar{n}$ was 0.35 and 0.56 for the 3.5×10^{-6} and 3.5×10^{-7} M s^{-1} feed, respectively. With the smaller, 57 nm, seed latex lower $\bar{n}$ values of 1.8×10^{-2}, 1.9×10^{-3} and 1.8×10^{-2} were determined for the feed conditions of 3.5×10^{-6}, 7.0×10^{-7} and 7.0×10^{-8} M s^{-1}, respectively.

Table 7
Feed and post-feed heat flow data, Q_r, for seeded styrene emulsion polymerizations using TBHP/Fe with reductant variations

Reductant	Feed Q_r (W)	Post-feed Q_r (W)
SFS	11.2, 9.51, 7.78	0.500, 0.654, 1.25
ASA	11.3,10.3,7.9	1.22,1.48,2.72
MBS	6.94, 10.34, 6.91	2.90, 1.17, 3.77

An example of the heat flow vs. time data for an initiator pulse is presented in Fig. 5 for the seeded polymerizations using the 103 nm unswollen diameter seed. The steady-state $\bar{n}$ values determined from this series of polymerizations are presented in Fig. 6, overlaid with the original data of Hawkett et al. [20]. The data in the present paper in this figure are for a system with particle size and particle concentrations very close to those of Hawkett et al. Data are plotted as a function of the entry rate coefficient ρ (the value of ρ from the data of Hawkett et al. are corrected from the original paper to take proper account of the fate of exited radicals [7,26]); an estimate for the entry rate coefficient for each initiator feed condition was made by assuming 100% entry efficiency. This assumption will be shown in the following section to be valid, and in fact expected, for hydrophobic radical initiation.

An interesting observation was apparent in this study: Significant retardation of the approach to steady state was observed in all experiments. This is seen in Fig. 5, with the approach to steady state taking several hundred seconds. Inhibition is usually supposed to arise from the very fast rate of reaction of radicals with oxygen relative to the rate of their propagation with monomer. In a typical emulsion polymerization of styrene, initiated with persulfate, radicals are formed in the aqueous phase where they have a significant residence time before entry, leading to ideal inhibition by oxygen. If instead the radicals enter with a greatly enhanced rate then this inhibition becomes a retardation, as observed with vinyl acetate [43]. In all the experiments performed in this section, the approach to steady state was much slower than expected upon the first initiator feed (Fig. 5). It was observed that this slow increase in rate was not seen when the initiator feed was commenced a second time. These observations are consistent with the retardation of polymerization due to the presence of residual oxygen in the reactor. The second feed period also implies that there is little oxygen being introduced by the redox feed by the rapid increase in rate upon commencement of the feed.

Molecular weight distributions were also measured the polymerizations under feed concentrations of 1×10^{-1}, 1×10^{-2} and 1×10^{-3}% (wt/wt) initiator. These are presented in Fig. 7, where each set of data has been has been normalized for comparison. These data will be used later for an alternative estimate of ρ.

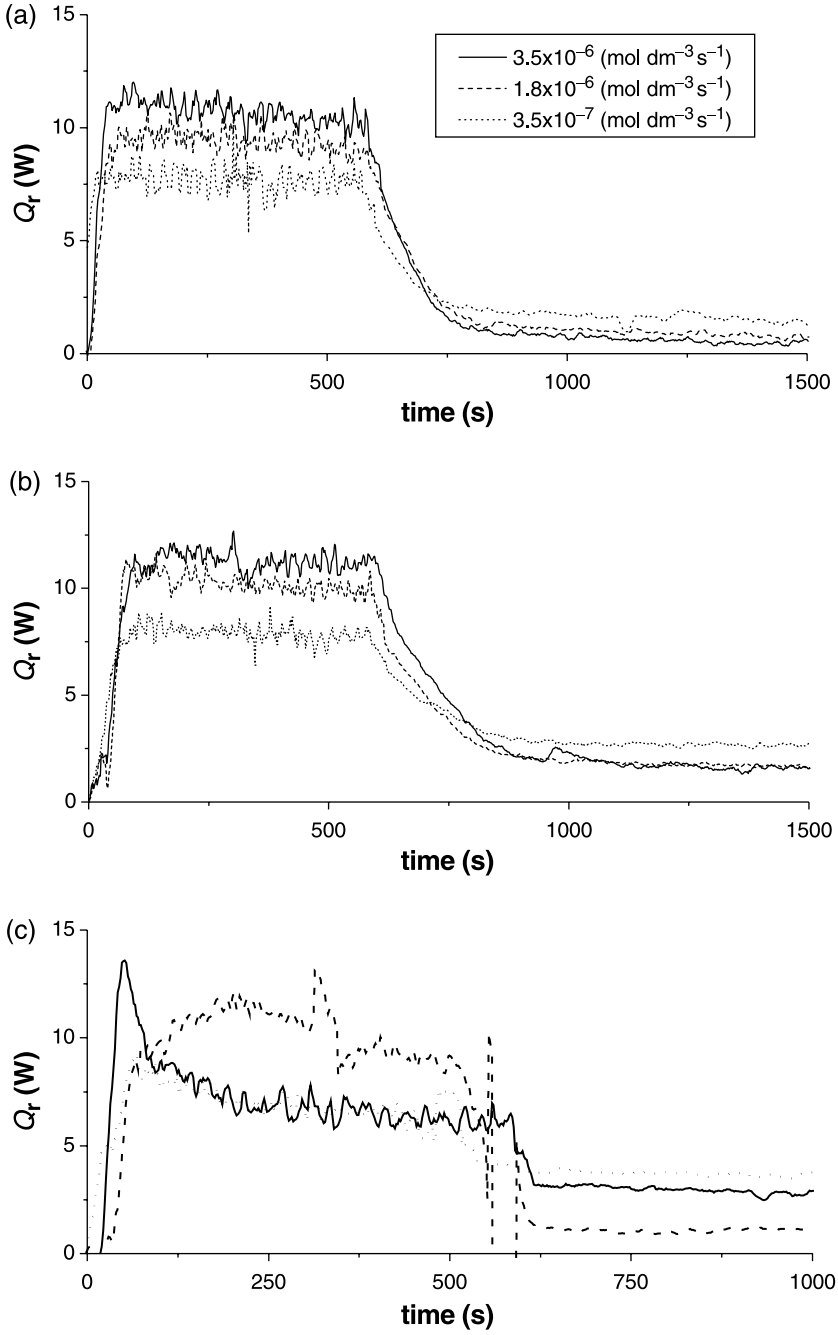

Fig. 3. Polymerization rate data (as reaction heat flows) for the seeded emulsion polymerization of styrene using TBHP/Fe initiation with: (a) SFS, (b) ASA and (c) MBS as reductant (initiator feed rates indicated by the legend).

5. Results: Aqueous-phase species

Using the initiation conditions of the successful styrene polymerizations given above, ab initio, surfactant-free polymerizations of MMA were performed as detailed previously. The reaction temperature profiles (which are proportional to the polymerization rate) are presented in Fig. 8. These data show that under initiation with SFS and ASA the system nucleated quickly and the reaction proceeded to completion within around 1500 s (with the Trommsdorff–Norrish gel effect seen as the sharp increase in rate between 1000 and 1500 s). The MBS system, however, proceeded at a reduced rate, taking around 6000 s for complete reaction, although it is not possible from these data to conclude if that is due to differences in N_p or a reduced radical flux. As these were ab initio polymerizations, these data do not conclusively shed much light on the particle growth kinetics but seem consistent with the previous results (Fig. 3) that showed MBS exhibiting poorer control than SFS and ASA.

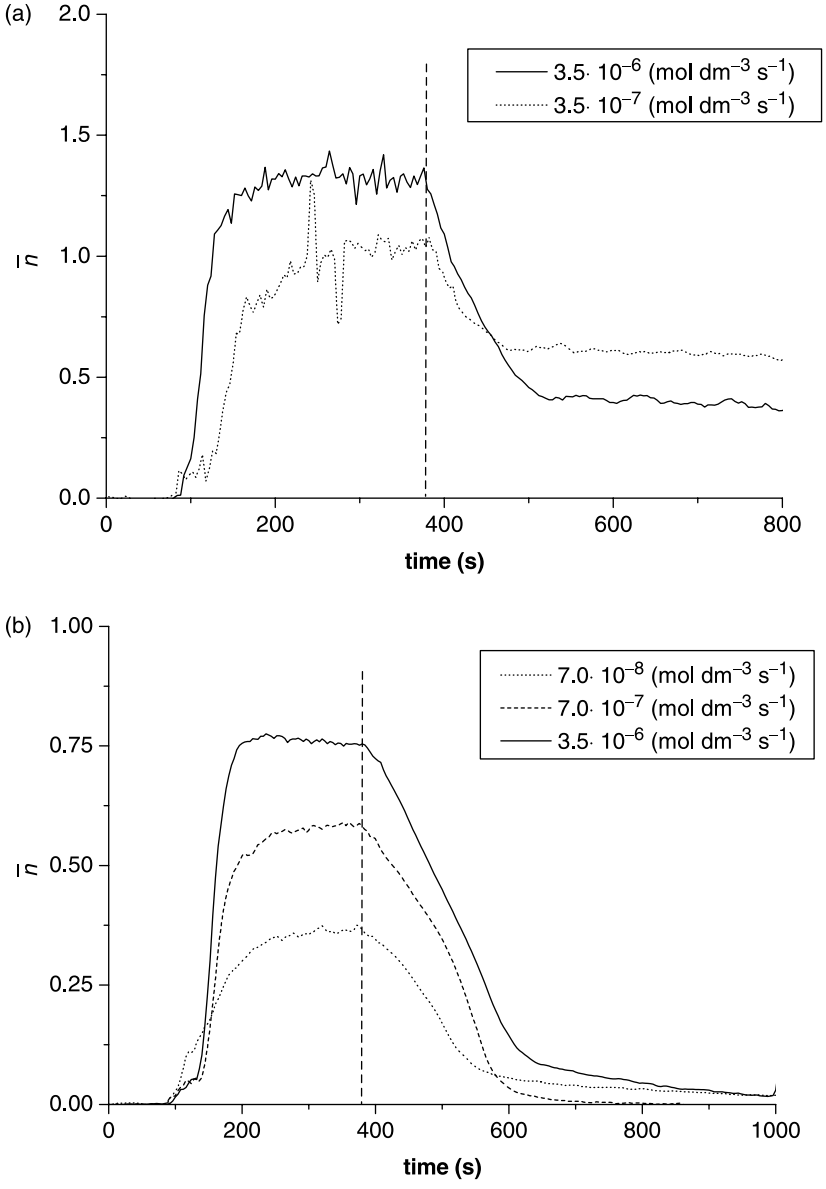

Fig. 4. $\bar{n}$ vs. time data for seeded styrene emulsion polymerizations with a fixed period of initiator addition (TBHP/Fe/SFS): (a) 127 nm unswollen diameter seed latex, (b) 57.2 nm unswollen diameter seed latex. Vertical dashed line indicates the end of initiation addition and the initiator feed rates are given in the legend.

A surprising but revealing result was found in those polymerizations which used SFS and MBS as reductants for the TBHP. Although the conditions were surfactant-free, and the suspected primary initiating radical was the *tert*-butoxy species, which is not expected to produce any in situ surfactant, latexes were formed that were colloidally stable for periods of up to several days. After such a time, the latex would settle but could be redispersed with agitation. Such stability was not observed with the ASA experiment, which when agitation was ceased would separate from a dispersed system into organic-rich and water-rich phases. Analysis of the aqueous phase by electrospray mass spectrometry showed that no detectable amounts of hydrolysis product of MMA (specifically methacrylic acid) were formed except under very harsh basic conditions, which implies that the observed colloidal stability is very unlikely to be due to the formation of electrosteric stabilizer from any such methacrylic acid. This suggests the formation of in situ surfactant during the reactions with SFS and MBS, arising from the formation of charged radical products by the reductant species that form oligomers to act as stabilizers for the polymer particles. ES/MS analysis of the latex aqueous phase was undertaken to identify such species.

5.1. Electrospray mass spectrometry analysis

Both positive and negative electrospray mass spectra of the aqueous phase were obtained in the case of initiation by

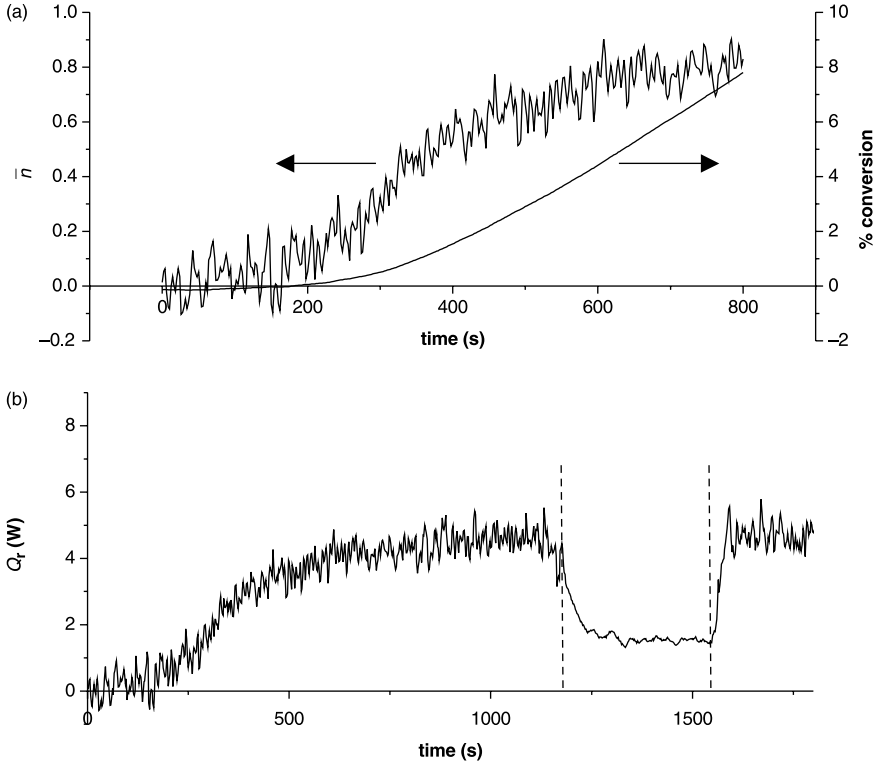

Fig. 5. (a) Conversion and $\bar{n}$ vs. time data for seeded styrene emulsion polymerization (example for feed concentration of 0.1%) under 'zero-one' conditions and (b) heat flow data for this reaction including the commencement of a second initiator pulse demonstrating no retardation upon second initiator pulse (vertical dashed lines indicate where initiator feed has been stopped and then restarted).

SFS; these spectra are given in Fig. 9. They show several distributions of singly charged MMA oligomers (evident by *m*/*z* separations of 100, the molecular weight of monomer) containing up to approximately nine monomer units. Due to the difficulty in obtaining sufficient signal-to-noise with negative-ion detection, only a positive-ion spectrum is reported for the MBS case. This is presented in Fig. 10(a) with major peaks at similar *m*/*z* to those observed for SFS with species up to 12 monomer units long. In both cases, species that consistently occurred with *m*/*z* spacing of 100 were identified as the oligomeric species of interest and an identification of their end groups was made. Fig. 10(a) shows a section of the SFS negative ion spectrum, showing major repeating peaks commencing at 167, 181 and 196, and minor peaks 30 45 and 61. Similarly Fig. 10(b) shows repeating peaks in the positive ion spectrum commencing from 405, 427, 441, 445, 447 and 473.

Fig. 10(a) shows the positive-ion spectrum for MBS. In

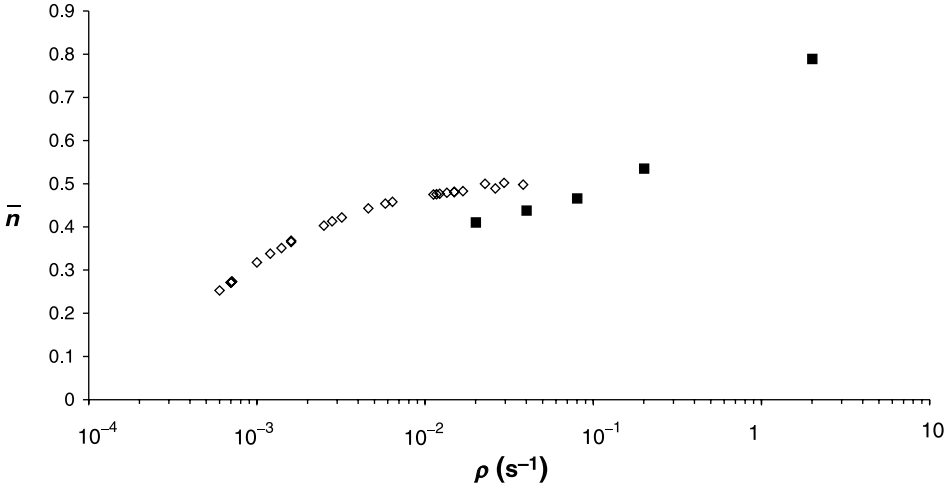

Fig. 6. $\bar{n}$ as a function of ρ for the redox initiated seeded styrene polymerizations of this study overlaid with those of Hawkett et al. (using 103 nm unswollen diameter latex and particle number similar to the Hawkett experiments).

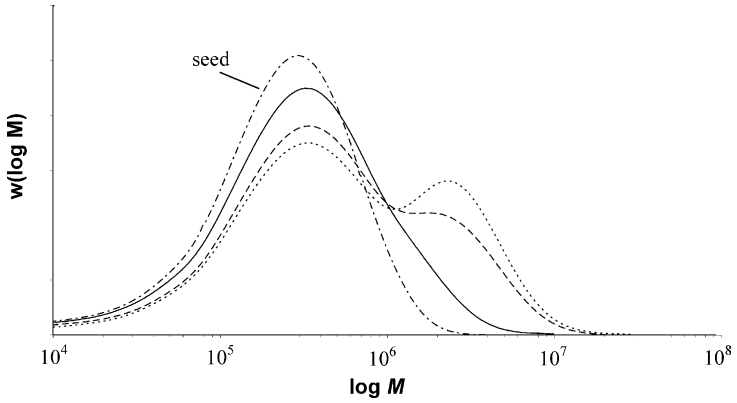

Fig. 7. (a) Molecular weight distributions for the 103 nm unswollen diameter polystyrene seed latex and seeded, zero-one emulsion polymerizations of styrene using redox initiator (redox feed concentrations: 10^{-1} (solid), 10^{-2} (dashed) and 10^{-3} (dotted) % (wt/wt)) and and (b) ln($P(M)$) plots for these data with the seed distribution subtracted.

this case a similar analysis to that undertaken for SFS resulted in similar major peaks being observed at integer multiples of 100 plus 7, 29 and 47. There were also recurring minor peaks at integer multiples of 100 plus 3, 4, 18, and 82.

Distributions of oligomer peaks such as observed for SFS and MBS were not seen for ASA (negative-ion spectrum shown in Fig. 10(b)). The major peaks observed in this spectrum occurred in two clear groupings: The first with a spacing of 100 between 276 and 577, and the second at higher *m/z* with separation of 143–144.

5.2. End group assignments

The radical products formed in the redox initiation of TBHP with SFS or MBS have not been definitively determined previously. Some plausible reaction schemes have been presented previously: One such suggestion is that HSO_3 end-groups are formed through transfer reactions [44] in bisulfite systems, and Makarov [45] proposed a

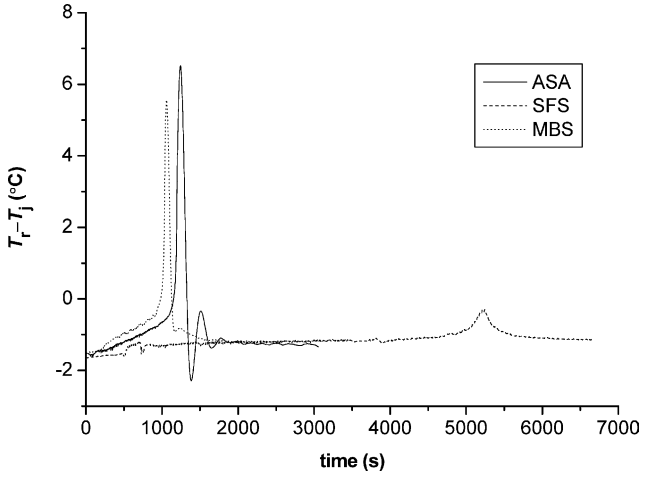

Fig. 8. Reaction temperature profiles (proportional to Q_r) for ab initio MMA emulsion polymerizations using TBHP/Fe with either SFS, ASA or MBS as reductant.

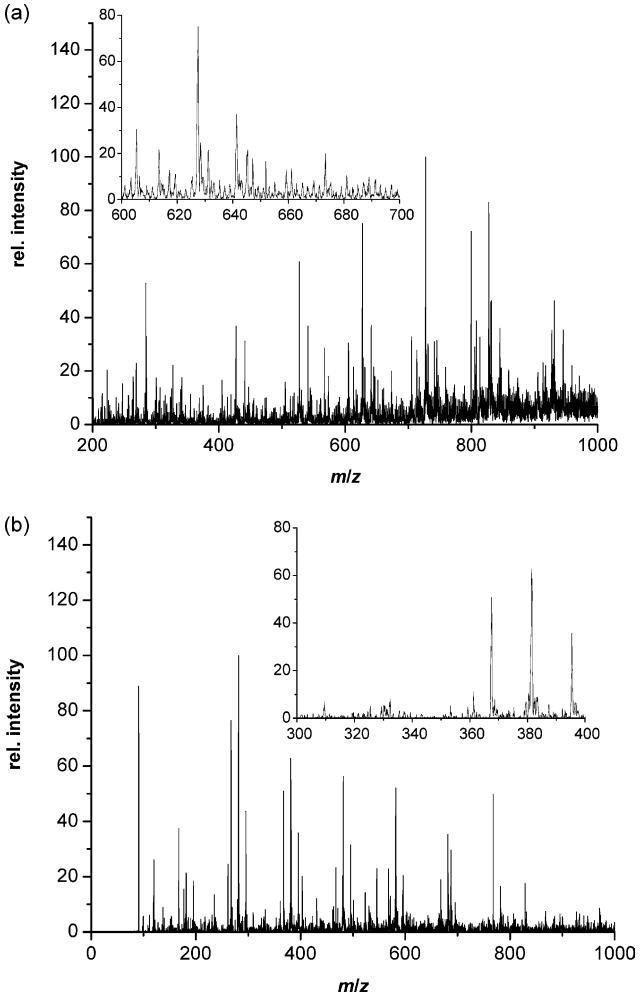

Fig. 9. ES/MS spectra for aqueous phase oligomeric products in the ab initio emulsion polymerization of MMA using TBHP/Fe/SFS initiation: (a) Positive ion detection, (b) negative ion detection. A representative distribution of recurrent peaks over an *m/z* interval of 100 is given in the inserts.

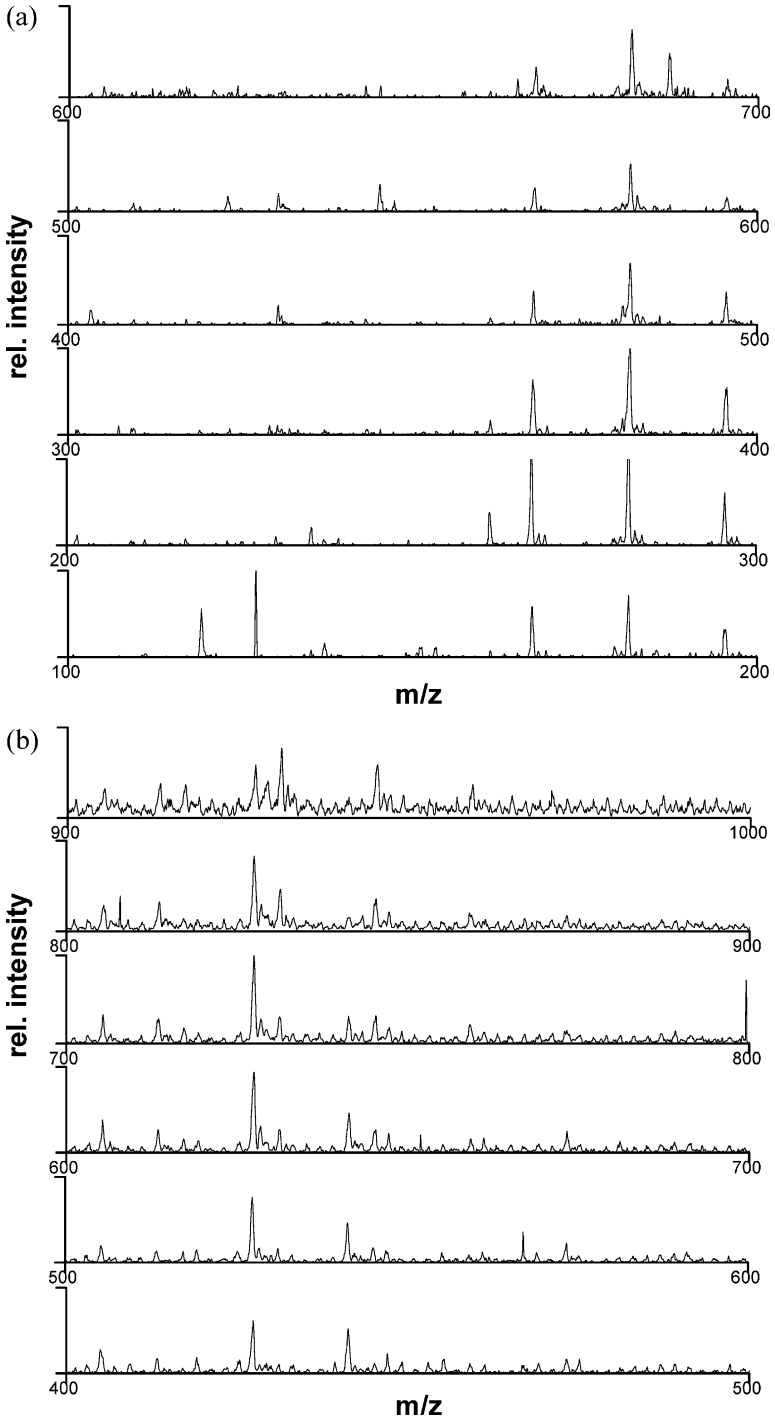

Fig. 10. Overlay of ES/MS data for ab initio emulsion polymerization of MMA using TBHP/Fe/SFS as initiator shown as overlaying sections with a range of 100 (in *m*/*z*): (a) Negative ion spectra for *m*/*z* from 100 to 700, (b) positive ion spectra for *m*/*z* from 400 to 1000.

mechanism for the decomposition of SFS in acidic conditions, involving the formation of the $SO_2^{-\cdot}$ radical anion. With these suggestions as a guide, a starting hypothesis is that the most plausible reactive species formed in the redox reaction of TBHP/Fe with SFS or MBS are $SO_2^{-\cdot}$ and/or $SO_3^{-\cdot}$ radicals, although other species such as $HOCH_2^{\cdot}$ may also be postulated to be formed. Other unreactive species such as SO_2, sulfate ions and formaldehyde may be formed as well.

Considering the SFS results, it is immediately apparent that oligomers initiated by a *tert*-butoxy radical and terminated by transfer or disproportionation (as is expected in the polymerization of MMA) would have molecular weights (plus integer multiples of 100) of 74 or 96 in the

positive-ion spectrum for species associated with H^+ or Na^+, respectively, (this species is not expected to be visible in the negative ion spectra). There is a minor peak visible at 73 and an even smaller peak at 95 but they are clearly not the major species observed. This result is in fact reasonable, as the water solubility of such an oligomer should be very low: A key point in the entry mechanism as discussed in the following discussion section.

A species with a single SO_2^- end group would appear at 64 in the negative ion spectra and 66 ($2H^+$), 88 (H^+, Na^+) and 10 ($2Na^+$) in the positive spectra. None of these peaks are visible in either spectrum as a major peak. However, a SO_3^- end group or a SO_2^- and OH end group pair yield masses that may explain the major species observed.

The small peak at 19 and the larger peak at 41 in the positive ion spectra also may be explained by considering a SO_2^- and a CH_2OH end group pair. These species should exhibit molecular weights of 97 ($2H^+$), 19 (H^+, Na^+) and 41 ($2Na^+$). Furthermore, this species should be seen at 95 in the negative ion spectrum. In fact all of these species are seen to be present in both spectra.

The major negative ion peak at 67 (as well as some minor peaks) still requires explanation, as do several significant positive ion peaks. The end groups postulated here cannot account for such masses.

Similar results were found for the MBS system as with the SFS system. The positive spectrum displayed peaks in the range of 3–7, 18, 29, 47, and 82 (plus integer multiples of 100). The fact that there were some repeating end groups found predominantly at lower molecular weights ($m/z < 800$), signals at 82 and 3–4, and others at higher molecular weights ($m/z > 500$), 7 and 29 implies two different processes. It was stated previously that the two end groups in a SO_2^- and OH pair and that for a single SO_3^- end group are almost coincident in molecular weight (differing only by a hydrogen atom). It is plausible then for this system that both SO_2^- and SO_3^- end groups are present. A further check is to look for a SO_3^- and OH end group pair. This would exhibit major peaks at 99 ($2H^+$), 21 (H^+, Na^+) and 43 ($2Na^+$). There are some low intensity peaks at molecular weights close to these, but it cannot be conclusively said that they are present.

The oxidation reaction(s) of ASA have not previously been definitively identified for such redox systems, although studies [46] using variable-sized microband electrodes have lead to suggestions of plausible reaction pathways for the double oxidation of ASA to dehydro-ascorbic acid. This process involves the formation of a radical anion that may be reactive to monomeric double bonds, and so there may also be the presence of reactive species formed by ASA which should be detectable by ES analysis.

For ASA, the sequence of short oligomers, observed for m/z values in the range 276–577 in the negative ion spectra, corresponds to MMA oligomers with an ASA group, as the molecular weight of ASA is 176 and MMA adds 100 for each repeat unit. This probably corresponds to an ASA end group being formed either by the propagation of an ASA radical formed through the redox process or by proton abstraction by a *tert*-butoxy radical from an ASA molecule. The distribution at higher m/z, however, does not yield to easy interpretation, partly because the spacings do not correspond to MMA units.

5.3. Summary of redox mechanism

It is apparent from the electrospray analysis and the observations of colloidal stability that several conclusions and postulates can be formed:

1. The absence of large populations of oligomers with *tert*-butoxy end groups implies that they are entering the latex particles with a high efficiency. Therefore, it can be postulated that the entry of these radicals occurs quickly on the timescale of aqueous-phase termination.
2. The colloidal stability observed without the addition of surfactant implies the production of hydrophilic radicals that are producing oligomers (at least for MMA) that can act as an in situ surfactant.
3. The hydrophilic species appear be present in the largest quantities for SFS and MBS systems. These observations can be justified by using the ES/MS data to infer that such species are formed by the propagation and termination of $SO_2^{-\cdot}$ and/or $SO_3^{-\cdot}$ radical species. Additionally, ASA appears to play a role in the aqueous-phase chemistry, and this may be due to the formation of radical species as the intermediate step in a two-step oxidation process.

6. Discussion: Aqueous-phase events and entry

Using the results of the previous sections it is possible to compose a model for entry under initiation by the redox systems used in this work. The principles used in composing this model are general and allow reasonable mechanisms to be deduced for most common redox initiators.

6.1. Entering species

It is assumed that TBHP reduces to a *tert*-butoxy radical which can propagate with aqueous-phase monomer (or enter a latex particle); however, the aqueous-phase analysis for the ab initio polymerizations of MMA given in the previous section show that there is initiation of monomer by radical species other than by the *tert*-butoxy radical. This is not an aspect of such systems that is often considered, and the effects of this initiation upon the kinetics of entry and the latex physical properties are examined here. These species, which will probably also be present in the corresponding styrene systems, can have significant physical effects upon the emulsion system, as demonstrated by the stability of the

latexes formed with SFS and MBS through the production of in situ surfactant. To ascertain the kinetic significance of these species requires the analysis of polymerization rate data for styrene.

Table 7 details the steady-state (during redox feed) and post-feed polymerization heat flows for styrene, determined calorimetrically for TBHP/Fe with each of the three reductants and this data is shown in Fig. 3. As discussed previously, MBS produced inconsistent and irreproducible kinetics and is not considered for the kinetic analysis (although the water-phase species produced by this system have been examined). The steady-state polymerization rate data collected using ASA and SFS as reductants show that the total polymerization rate during the initiator was not significantly affected by the choice of either species, although there were some significant differences in the post-feed period, which will be discussed later. These results are consistent with the supposition that the *tert*-butoxy radical is the dominant initiating species, which we conjecture is due to a markedly faster and more efficient entry process than those of the other species formed in the redox process. In order to justify this claim, we consider the efficiency of radical capture in an emulsion system containing hydrophobic and hydrophilic radicals in the water phase.

6.2. Radical capture efficiency

It is reasonable to assume that the *tert*-butoxy radical is quite hydrophobic (although the carbon–oxygen bond would be expected to have a small associated dipole) and hence should enter latex particles by a barrierless process at the diffusion-controlled limit: The special case of the Maxwell–Morrison model with $z=1$. This contrasts with the entry kinetics of the radical species proposed to form from the reductant species above. The radicals produced by SFS and MBS, being charged, or from ASA, being hydrophilic, should exhibit Maxwell–Morrison kinetics with $z>1$, and hence enter with a significantly lower efficiency, due to the requirement for propagation prior to entry leading to enhanced aqueous-phase termination. The following section will explore this postulate that the *tert*-butoxy radicals enter particles with 100% efficiency and hence that the rate data may be interpreted by making the assumption that the entry rate can be found simply by equating to the feed rate of initiator per particle (under steady-state conditions).

The aqueous-phase radical production rate is now quantified for the TBHP/SFS system. If the approximation is made that a single radical species is formed from SFS, labeled S, and this can only terminate in the aqueous phase and further, that *tert*-butoxy radicals, labeled T, can either enter latex particles (at the diffusion limit) or terminate with other radicals in the aqueous phase, then an estimation of the capture efficiency of T species can be made (which by only allowing S radicals to terminate should in fact form a lower bound for efficiency).

Under steady-state conditions, S radicals are produced at a rate equal to the rate of addition of initiator, and terminate with other S radicals, leading to:

$$\frac{\mathrm{d[S]}}{\mathrm{d}t} = \phi - 2k_{\mathrm{t,aq}}[\mathrm{S}]^2 \tag{3}$$

Here ϕ is the rate of radical production, assumed to be the feed rate under the steady-state conditions considered here, and $k_{\mathrm{t,aq}}$ is the bimolecular termination rate coefficient for two monomeric-like radicals in the aqueous phase. This result assumes that, for S radicals, the effect of entry is small compared to aqueous-phase termination (assuming these radicals exhibit similar physical properties to a sulfate radical). This assumption, which is also made in the Maxwell–Morrison treatment [6] in order to obtain a simple analytical solution (although not part of the physical model, this is found usually to be a good approximation), immediately gives the steady-state concentration of S radicals in the aqueous phase:

$$[\mathrm{S}] = \left(\frac{\phi}{2k_{\mathrm{t,aq}}}\right)^{1/2} \tag{4}$$

The fates of T radicals are now considered. In the same manner as for S radicals, the T radicals are considered to be produced at a rate equal to the feed rate, and may terminate in the aqueous phase with S radicals. The only other mechanism to consider is entry. Using the arguments proposed earlier in this section, it is reasonable to assume that T radicals may enter particles (without aqueous-phase propagation) at diffusion-controlled rates. The evolution equation for T radicals is thus:

$$\frac{\mathrm{d[T]}}{\mathrm{d}t} = \phi - k_{\mathrm{diff}}[\mathrm{T}]\frac{N_{\mathrm{p}}}{N_{\mathrm{A}}} - 2k_{\mathrm{t,aq}}[\mathrm{S}][\mathrm{T}] \tag{5}$$

where k_{diff} is the diffusion coefficient for a monomeric-like species in the aqueous phase. The diffusion-controlled model is used for $k_{\mathrm{t,aq}}$ and k_{diff}:

$$k_{\mathrm{diff}} = 4\pi \mathrm{D_W} r_{\mathrm{s}} N_{\mathrm{A}} \tag{6}$$

$$k_{\mathrm{t,aq}} = 8\pi p D_{\mathrm{W}} r_{\mathrm{r}} N_{\mathrm{A}} \tag{7}$$

Here D_{W} is the diffusion coefficient for monomer in the aqueous phase (taken as $3.5\times10^{-5}\,\mathrm{cm^2\,s^{-1}}$), r_{s} is the swollen particle radius, and the interaction distance, r_{r}, is that for a radical–radical encounter, taken as 0.6 nm [47]. The probability term, $p=1/4$, is required to account for radical spins [48]. The entry probability per T radical is then:

$$P_{\mathrm{entry}} = \frac{k_{\mathrm{diff}}\frac{N_{\mathrm{p}}}{N_{\mathrm{A}}}}{k_{\mathrm{diff}}\frac{N_{\mathrm{p}}}{N_{\mathrm{A}}} + 2k_{\mathrm{t,aq}}[\mathrm{S}]} \tag{8}$$

The concentration of T radicals can now be calculated and entry efficiency estimated. Using $\phi = 3.5\times10^{-6}\,\mathrm{M\,s^{-1}}$

(taken from experimental feed conditions) and a swollen particle radius of 43 nm produces a value for the probability of entry $P_{entry}=0.98$ (equivalent to entry efficiency), consistent with the hypothesis made previous in this discussion that *tert*-butoxy radicals under these redox conditions should exhibit a high efficiency.

The capture efficiency for S radicals entering by the Maxwell–Morrison mechanism can also be estimated, as this process of radical entry (for charged, hydrophilic initiators) is well understood. The Maxwell–Morrison mechanism for entry describes a process whereby the hydrophilic radical must propagate to a critical degree of polymerization, denoted z, before reaching sufficient surface activity to irreversibly enter a latex particle. In this manner the pseudo-first-order rate coefficient for entry, ρ, can be calculated, as well as the initiator efficiency, using knowledge of aqueous-phase propagation and termination kinetics in conjunction with knowledge of the free energy of solvation of the water-phase oligomers. The result is:

$$\rho \approx \frac{2k_d[I]N_A}{N_p}\left\{\frac{\sqrt{k_d[I]k_{t,aq}}}{k_{p,aq}C_W}+1\right\}^{1-z} \tag{9}$$

where k_d and $k_{p,aq}$ are the rate coefficients for initiator decomposition and aqueous phase propagation, respectively, and [I] is initiator concentration. An extension of Eq. (9) for redox systems can be made by replacing the rate of production of radicals by thermal decomposition, $2k_d[I]$, with the rate of addition of redox initiator, ϕ. This gives the equivalent expression for ρ:

$$\rho \approx \frac{N_A}{N_p}\phi\left\{\frac{\sqrt{\phi k_{t,aq}}}{4k_{p,aq}C_W}+1\right\}^{1-z} \tag{10}$$

which in the limit of $z=1$, as applicable for hydrophobic initiating radicals, takes the form:

$$\rho_{diff} = \frac{N_A}{N_p}\phi \tag{11}$$

This is now used to estimate the efficiency of entry for a charged S species. Using the feed rate and aqueous termination rate coefficient given previously together with the saturated water phase concentration for styrene ($C_W^{sat}=1\times10^{-3}$ M [30]), the established value for z for styrene and persulfate initiator ($z=2$—this assumes that the ionic species has a single change and is hydrophilic, like SO_4^-; note that the value of z is different for more hydrophobic initiating entities [5]), the aqueous phase propagation rate coefficient ($k_{p,aq}=4k_p$ M^{-1} s^{-1} [7,49]) and a typical experimental value for N_p (5×10^{16} dm^{-3}), the initiator efficiency is calculated to be approximately 10%. It is fortuitous to note for the purposes of this study that the choices for parameters such as $k_{p,aq}$ are not overly critical as reasonable changes to these numbers do not drastically affect either the efficiency of the diffusion-limited entry of hydrophobic radicals or the comparison of their entry rates with the hydrophilic radicals. Hence under typical redox initiation conditions, entry of hydrophilic radicals will not be significant when compared to that of the hydrophobic radicals.

6.3. Redox entry rates

Working with the model for entry described above for systems such as TBHP/SFS, where entry is dominated by hydrophobic species entering with approximately 100% efficiency and hydrophilic radicals do not significantly participate, calorimetric data for seeded styrene emulsion polymerizations can now be studied.

6.3.1. 127 nm seed

The $\bar{n}$ results from the pulsed polymerizations of the 127 nm seed latex (Fig. 4) show that, since $\bar{n}$ is above 0.5, particles of this size are not described by zero-one kinetics under the experimental conditions used in this work. This system is better described by the zero-one-two model [22,23,50] or pseudo-bulk kinetics. The pseudo-bulk approximation without exit may not be appropriate, as the steady-state value for $\bar{n}$ is not consistently proportional to the square root of the entry rate (assuming the entry rate is proportional to the feed rate and a constant termination rate). The pseudo-bulk equation for $\bar{n}$ in the steady-state is:

$$\bar{n}_{ss} = \sqrt{\frac{\rho}{2c}} \tag{12}$$

Here $c=\langle k_t\rangle/N_AV_s$ is the pseudo-first-order rate coefficient for termination, where $\langle k_t\rangle$ is second-order termination rate coefficient averaged over all chain lengths of propagating radicals [48] and V_s is the swollen volume of the particle. If ρ is determined by dividing the feed rate ($M\,s^{-1}$) by the particle concentration (M), application of the pseudo-bulk steady state equation yields average termination rate coefficients of 2.4×10^7 and 3.2×10^6 M^{-1} s^{-1} using the rate data for the two feeds. These values are inconsistent if entry is always proportional to feed rate (particle number and w_p are effectively the same), $\langle k_t\rangle$ is constant and there are no artifacts of the initiator. However, these values for $\langle k_t\rangle$ are still both physically reasonable when compared to experimental determinations such as those of Clay et al. [51], and $\langle k_t\rangle$ has a radical flux dependence that is consistent with the trend in these two data. This can be seen by simulating the expected $\langle k_t\rangle$ for each of the two radical fluxes using the methods of Clay et al. [51] using the standard parameters for styrene at 50 °C (Table 8). These simulations show that the trends as well as the magnitudes observed experimentally for $\langle k_t\rangle$ as a function of radical flux (using the feed rate as the radical creation rate under steady-state conditions) are consistent with these simulated values.

6.3.2. 57.2 nm seed

The $\bar{n}$ vs. time plots of Fig. 4 for the smaller particle

system show two interesting phenomena. Firstly, the most concentrated feed resulted in an apparent $\bar{n}$ greater than 0.5. Particles of this size (swollen radius of 41 nm) under conventional initiation conditions, and corresponding entry rates, should be approximated well by the zero-one model. However, for entry rates exceeding those normally accessible, such a departure is not unreasonable nor is it unexpected. The following section will demonstrate that under the assumption of highly efficient entry for hydrophobic radicals, this result is consistent with what is expected by the Smith–Ewart treatment of particle kinetics.

The seed latex was sized by light scattering which, as mentioned previously, displays a bias towards larger particle sizes. Thus the number-average size, needed to determine $\bar{n}$, may be slightly but significantly oversized by the PCS. An approximate 10% overestimation of particle size leads to an approximate 30% overestimation of $\bar{n}$. Such an overestimation takes the observed $\bar{n}$ values from 0.75, 0.55, and 0.37 to 0.55, 0.40 and 0.27, respectively. There is also expected to be some degree of error associated with $\bar{n}$ through the choice of C_p. It was assumed in this analysis that C_p^{sat} should take a value of 5.5 M; this value was used unless the conversion implied that the systems had entered interval 3 (the emulsion polymerization region in the absence of monomer droplets) and so C_p had fallen to a value lower than this. In this case the lower calculated value was used. In order to interpret these data an analysis of expected kinetics will be presented by the application of the Smith–Ewart treatment (Fig. 11).

The results for $\bar{n}$ may be analyzed by means of the Smith–Ewart equations, to see if an $\bar{n}$ greater than 0.5 were possible with the redox entry rates used experimentally; while this treatment does not take into account chain-length-dependent termination kinetics, it has been shown [23] that this should not be in gross error in estimating a steady-state value of $\bar{n}$ for such a system. The method of Ballard [21] was employed to solve these equations as functions of ρ, k, c and the fate of exited free radicals. With the feed rate used to characterize ρ, suitable values for the exit rate coefficient, k, were calculated by assuming that all exited radicals re-enter the particles and remain there: Limit 2a exit kinetics [7]. The value for the average termination coefficient was varied between the values suggested to be reasonable in the work of Clay and Gilbert [51]. A second set of calculations was also performed with a reduced $\bar{n}$ based upon an assumed 10% experimental overestimation of particle size. The parameters used are given in Table 9 and the results presented in Fig. 12 for particle sizes (a) as inferred from PCS and (b) reduced by 10%.

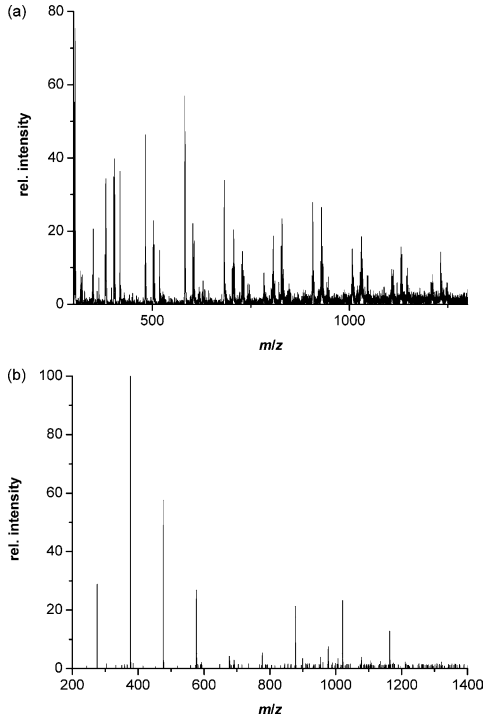

Fig. 11. ES/MS spectra for aqueous phase products in the ab initio emulsion polymerization of MMA using TBHP/Fe initiation: (a) Positive ion detection with MBS as reductant, (b) negative ion detection with ASA as reductant.

These calculations show values for $\bar{n}$ of 0.45 (for case (a), PCS sizing) and 0.42 (case (b), reduced size), taken as averages across all choices for c, at the lowest initiator feed rate. These are both higher than the experimental results of 0.37 for case (a) and 0.27 case (b). This suggests that the PCS sizing is a better representation, giving closer agreement between both the calculated and experimental value. Under the highest initiator feed rate conditions, the experimental data for $\bar{n}$ were 0.75 for case (a) and 0.55 for case (b). Physically reasonable parameters of $\langle k_t \rangle = 1 \times 10^6$ and $5 \times 10^6\ M^{-1}\ s^{-1}$ yield values for $\bar{n}$ using the Smith–Ewart treatment of 0.54 and 0.52 for case (a) and (b) using the former value for $\langle k_t \rangle$ and 0.71 and 0.62 for case (a) and (b) using the latter value for $\langle k_t \rangle$. Finally the intermediate feed experimentally showed $\bar{n}$ values of 0.55 (a) and 0.40 (b) and the corresponding calculated values were 0.50 (a) and 0.49 (b) for $\langle k_t \rangle = 5 \times 10^6\ M^{-1}\ s^{-1}$ and 0.54 (a) and 0.51 (b) for $1 \times 10^6\ M^{-1}\ s^{-1}$. These results also suggest that the

Table 8
Experimental and predicted $\langle k_t \rangle$ for the initiator feed rates (equivalent to radical flux) used in the seeded styrene polymerizations of the 127 nm unswollen diameter polystyrene seed latex

Feed rate ($M\ s^{-1}$)	$\langle k_t \rangle$ ($M^{-1}\ s^{-1}$, theory)	$\langle k_t \rangle$ ($M^{-1}\ s^{-1}$, experiment)
3.5×10^{-6}	4.8×10^7	2.4×10^7
3.5×10^{-7}	5.9×10^6	3.2×10^6

Data given for initiator feed rates of 3.5×10^{-6}, 1.8×10^{-6} and $3.5 \times 10^{-7}\ M\ s^{-1}$, respectively.

Table 9
Parameters used in the calculation of $\bar{n}$ for polymerizations using the 57 nm polystyrene seed latex and also reproduced for 10% reduction in latex diameter (note: It has been assumed that exited radicals undergo complete aqueous-phase termination)

Parameter	$r_s = 40.1$ nm	$r_s = 37.0$ nm
ρ (s^{-1})	4.24, 0.828, 0.0828	3.09, 0.619, 0.0619
k (s^{-1})	1.78×10^{-2}	2.23×10^{-2}
k_t ($M^{-1}\,s^{-1}$)	1.0×10^{7}, 5.0×10^{6}, 1.0×10^{6}, 5.0×10^{5}, 1.5×10^{5}	1.0×10^{7}, 5.0×10^{6}, 1.0×10^{6}, 5.0×10^{5}, 1.5×10^{5}
c (s^{-1})	59.3, 29.7, 5.93, 2.97, 0.80	79.1, 39.5, 7.91, 3.95, 1.19

PCS sizing is more appropriate by a more consistent agreement across the feed regimes between the experimental value and the calculated value.

These results tentatively imply that the value for $\bar{n}$ at the highest feed rate exceeding 0.5 is not an artifact of particle size error and are not unreasonable observations. This conclusion has been reached upon the basis of the assumption that high initiator efficiency is observed for *tert*-butoxy radicals and numerical solutions to the Smith–Ewart equations (including variations in particle size). The use of high radical fluxes to push past the $\bar{n} = 0.5$ plateau is pursued further later in this work.

6.4. Redox initiation rate coefficients

The results presented in the previous section showed an interesting feature: After the redox initiator feed was switched off, the concavity of the rate data was initially the opposite to that expected (as mechanistically predicted for a sudden stoppage in initiation and as observed in γ relaxation data [49]) if initiation had ceased, such as observed in Fig. 4. The calorimetric determination of steady-state polymerization rates (or other slowly evolving processes) and of integrated quantities (such as total evolved heats for conversions) is well understood but the study of more dynamic processes by this technique has not received as much study. It was decided to determine both (a) if the data collected when the feed of initiator is turned off can shed light upon the redox and polymerization processes and (b) if in fact there are limitations to the dynamic response of the reaction calorimeter.

Usually when examining relaxation behaviour, such as by γ radiolysis, it is assumed that there is an instantaneous cessation in initiation. With a redox-initiation system, initiation may not stop instantaneously when the feed is stopped, and an estimate of the rate of radical production may be needed to interpret the observed rate of radical loss. We now model the effect of allowing a zero-one system to relax with a time-dependent loss of radical flux to determine if an estimate of the phenomenological redox rate

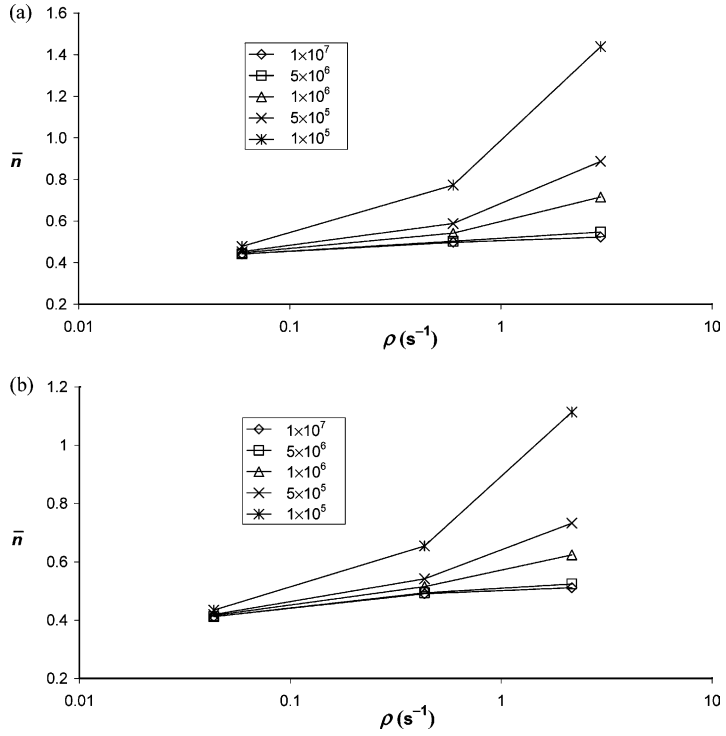

Fig. 12. (a) Calculated $\bar{n}$ (using the method of Ballard [21]) as a function of ρ for a range of $\langle k_t \rangle$ values (indicated in legend): (a) 57 nm diameter polystyrene seed latex ($r_s = 41$ nm) and (b) for 10% reduced diameter polystyrene seed latex.

coefficient can be made and if the concavity observed is physically reasonable.

For this purpose, an initial estimate for the rate of reaction of TBHP with Fe^{2+} is required. There have been values of the order of $10^2\,M^{-1}\,s^{-1}$ reported in the literature, for a range of similar hydroperoxides, such as in the work of Walling [52] and of Orr and Williams [53]. The later provides a value for the rate coefficient of this reaction with Fe^{2+}, for hydrogen peroxide at 50 °C, of approximately $150\,M^{-1}\,s^{-1}$.

These estimates allow the evolution equations for this redox-initiated zero-one system (with negligible spontaneous entry) to be modeled. The equations to solve for $\bar{n}$ then become, in the case of first order loss:

$$\frac{d[I]}{dt} = \phi - k_{diss}[I] \tag{13}$$

$$\frac{d[I^{\cdot}]}{dt} = k_{diss}[I] - k_{entry}[I^{\cdot}] \tag{14}$$

$$\frac{dN_0}{dt} = (\rho + k)N_1 - \rho N_0 \tag{15}$$

$$\frac{dN_1}{dt} = \rho N_0 - (\rho + k)N_1 \tag{16}$$

where

$$\rho = k_{diff}[I^{\cdot}] \tag{17}$$

$$k_{entry} = k_{diff}\frac{N_p}{N_A} \tag{18}$$

The analogous equations for limit 2a are also solved with the same initiator equations. The exit rate coefficient for either limit 1a (compete aqueous phase termination) or limit 2a (complete re-entry, no re-exit) can be estimated from the Maeder and Gilbert treatment [24]. For the 57 nm seed latex the predicted values for complete aqueous phase termination of exited radicals are $k_{ct} = 1.32 \times 10^{-2}\,s^{-1}$, and for complete re-entry, are $k_{cr} = 1.78 \times 10^{-2}\,s^{-1}$. These equations were solved numerically. Fig. 13(a), the calculation for which assumed limit 1a kinetics, shows that a long period of initiator decay is reflected in $\bar{n}$ by producing a relaxation shape similar to that seen in Fig. 4. However, the experimental results show a much faster relaxation in $\bar{n}$ than this calculation. Exploration of the kinetics was pursued with both the value for k_{diss} of $150\,M^{-1}\,s^{-1}$ and an increased value of $1500\,M^{-1}\,s^{-1}$ to establish the effect of an order of magnitude increase in this rate coefficient. Fig. 13(b) shows the profiles for [TBHP] and $\bar{n}$ (again assuming limit 1a) for $k_{diss} = 1500\,M^{-1}\,s^{-1}$. These calculations show that, for a sharper decrease in initiator concentration, the values for $\bar{n}$ also fall at a rate closer to that seen experimentally. It should be noted that the calculated relaxation behaviour of $\bar{n}$ still displays the unusual curvature seen in experiment early in the relaxation, albeit to a small extent.

Calculations were then performed using both exit limits for comparison with the experimental data, for the two lower feed concentrations that exhibited an $\bar{n}$ below 0.5. Fig. 14(a) shows the experimental $\bar{n}$ values for the lowest feed concentration and those calculated for $k_{diss} = 150\,M^{-1}\,s^{-1}$. Fig. 14(b) shows the same data but for $k_{diss} = 1500\,M^{-1}\,s^{-1}$. The lower value for k_{diss} does not fit the experimental result at all well for the post-feed period, whereas the relaxation calculated using the 10-fold increase in k_{diss} gives a better result. In this case the limit 2a system, which is the expected limit in these styrene systems, fits the approach to steady state and the first part of the relaxation. The limit 1a calculation appears to show that $\bar{n}$ is too low but again shows, qualitatively, a reasonable fit to the relaxation.

Fig. 14(c) and (d) shows the same calculation for the mid-strength initiator feed. As with the previous system, the approaches to steady state are similar to the experimental results. Also, as with the previous result, the literature value for k_{diss} fails dramatically to reproduce the observed radical loss. With the increased value of k_{diss}, the limit 2a radical loss kinetics do not provide a good fit to the late time relaxation data but do exhibit similar kinetics at early times. The initial slopes of the two calculated curves, particularly for limit 1a, show that this choice of k_{diss} may be overestimating the true value.

There are two possible conclusions that can be drawn from these calculations. (1) The first possibility is that the unusual curvature in the relaxation data is due to the non-instantaneous cessation of initiation when the feed is turned off. Thus the qualitative agreement of limit 1a to experiment, in so far as fitting the sharp radical loss, is a true reflection of the kinetics. Based upon the diffusion-controlled entry arguments made in this work, this implies that termination of exited radicals must occur by reaction with a non-radical species to yield a slow-reacting species, and/or through a redox reaction. This seems unlikely, however, as an accumulation of such a species would be evident throughout the course of the experiment and lead to an increasingly reduced rate. This is clearly not the case due to the ability to generate sustained steady-state polymerization rates (e.g. as in Fig. 2). (2) The second possibility is that the early time fit to experiment of limit 2a might be a better representation of the exit kinetics and the drop off after the first hundred seconds may suffer some influence of artefacts of the RC1 measurement. There is an unexplored possibility that the timescale for the radical loss is such that the RC1 cannot be used to follow it reliably. It was observed that the timescale of the relaxation for the calibration procedure (using the 20 W calibration heater) was approximately 90 s. As the smaller heat flows of these experiments should result in a quicker recovery, and this relaxation should be concave up, it is most likely that this process does significantly alter the data. However, it is not possible at this stage to definitively choose between these two alternatives

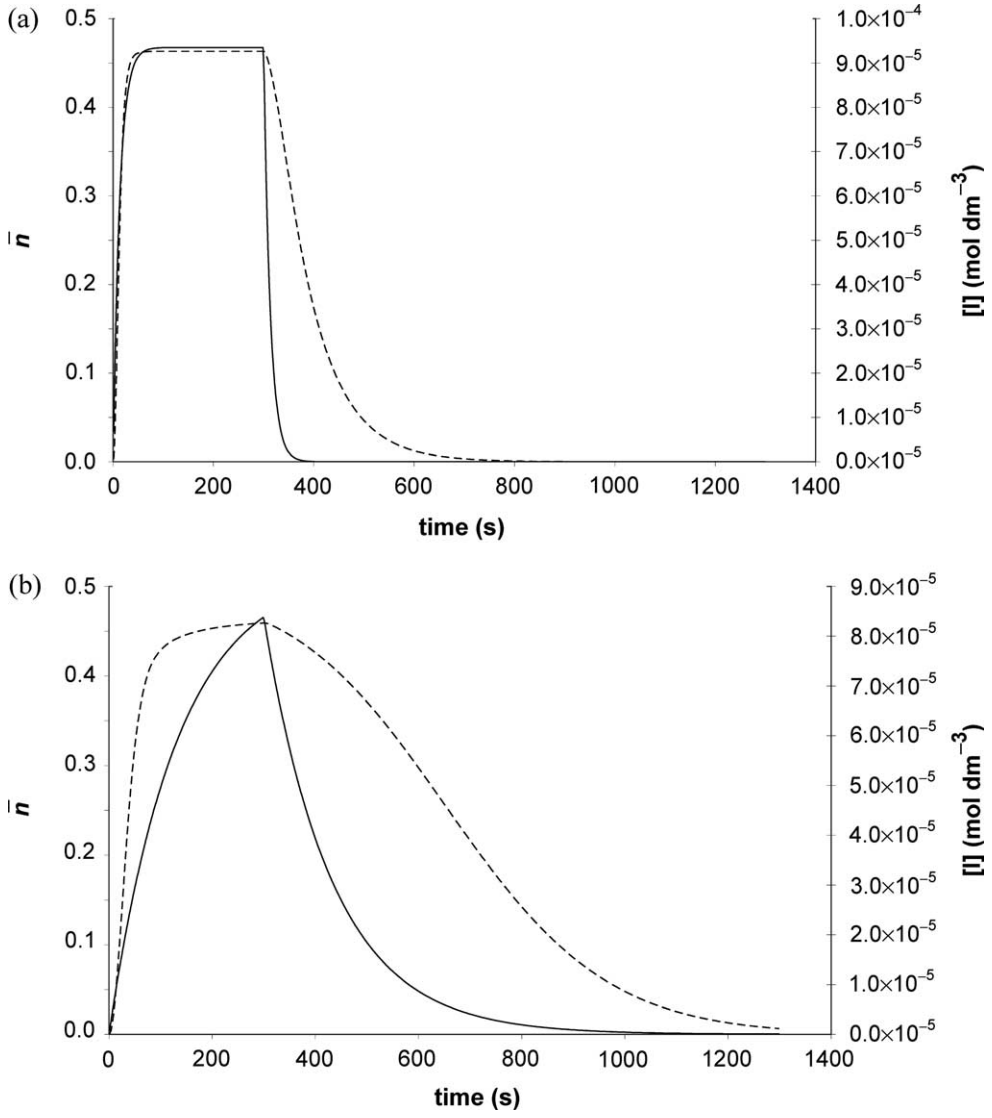

Fig. 13. Effect of assumed value for initiator decomposition rate constant (k_d) on simulated zero-one kinetics (with first-order radical loss). $\bar{n}$ (broken line) and initiator concentration (as [TBHP] in M, solid line): (a) $k_d = 150\ M^{-1}\ s^{-1}$, (b) $k_d = 1500\ M^{-1}\ s^{-1}$.

solely from these results. Experimental parameters, such as the amplification power of the RC1 cooling, could be used to test for such artefacts with further experimental work.

The second conclusion is that the literature value for the rate coefficient for reaction of TBHP with Fe(II) appears to significantly underestimate the true value for this quantity, at least under the experimental conditions of this section. The literature results were made at a higher pH than that used in these experiments and the reaction was monitored by physical sampling and iron detection by addition of α,α'-bipyridyl. The reaction also contained acrylonitrile to 'remove' radicals once they were produced. It would be suggested, as useful future work, to use an improved technique such as stopped-flow analysis to determine this rate coefficient at a range of pH values.

7. Discussion

7.1. Entry mechanism and polymerization kinetics

Having established a model for the mechanism and kinetics of redox initiation in seeded styrene emulsion polymerizations it was desired to test this entry model by studying the transition from zero-one to pseudo-bulk kinetics. In order to perform this study a system was chosen that meet two criteria: Firstly the experimental conditions (such as particle size and number) were the same as previous studies using tried and tested conditions and techniques, and secondly the particle size was such that a transition through these kinetic regimes was expected to occur for the entry rates employed previously in this work using redox initiator. It should be noted that, although it is expected, an actual experimental study of a seeded styrene emulsion

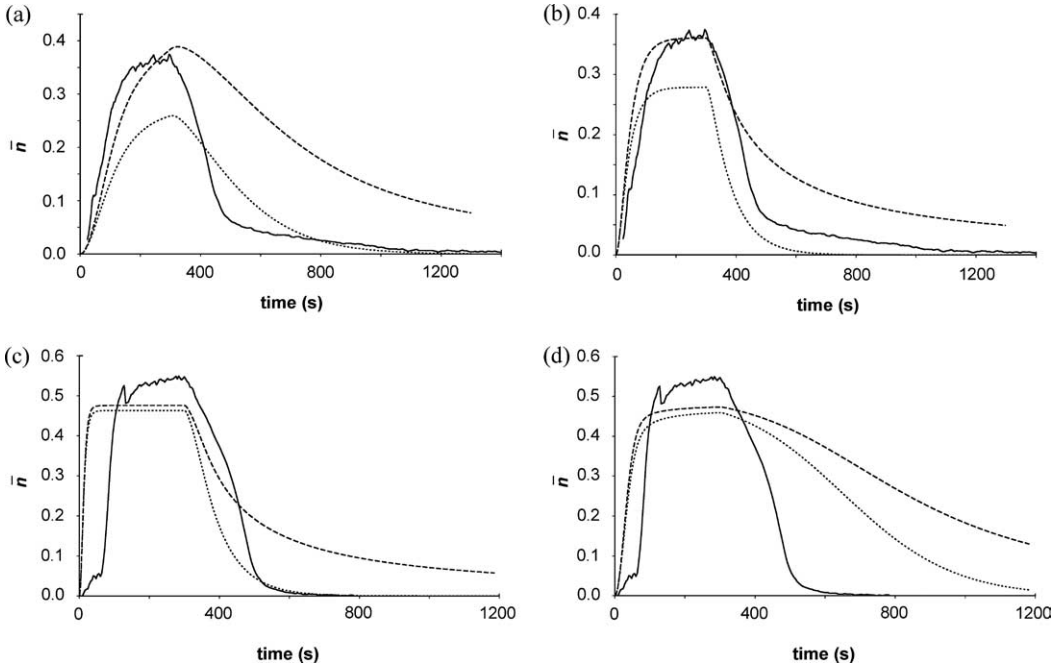

Fig. 14. Experimental and simulated $\bar{n}$ data for seeded zero-one styrene polymerizations (using 57.2 nm diameter seed latex) under pulsed redox initiation: (a) and (b) lowest feed rate using limit 1a (dotted) and limit 2a (dashed) models for exit, $k_d = 150$ and $1500\ M^{-1}\ s^{-1}$ in (a) and (b), respectively, (c) and (d) intermediate feed rate using limit 1a (dotted) and limit 2a (dashed) models for exit, $k_d = 150$ and $1500\ M^{-1}\ s^{-1}$ in (c) and (d), respectively.

polymerization moving from the zero-one regime into zero-one-two and pseudo-bulk kinetics is both novel and a direct consequence of the entry mechanism proposed in the previous sections.

The fundamental studies on the kinetics of styrene emulsion polymerization kinetics [20] used a seed latex which was fortuitously colloidally stable at very high ionic strength (and hence high concentrations of persulfate initiator), enabling use of persulfate concentrations of up to 8.33×10^{-2} M. At this initiator concentration an entry rate coefficient of $3.83\times10^{-2}\ s^{-1}$ at 50 °C, or in dimensionless form, a value of ρ/k of approximately 30, was observed, with an initiator efficiency of 1%. For the particle size used in these experiments (swollen particle radius of 79 nm) this value of ρ (and those leading up to it) exhibited the plateau for steady-state $\bar{n}$ at 0.5 as is predicted using the zero-one model (these values are reproduced in Fig. 6). Modeling of the kinetics with well accepted treatments of entry, exit and termination [5,7,23,54] show that is impossible to obtain sufficiently higher entry rates from persulfate initiation under these experimental conditions to go beyond $\bar{n} = 1/2$ for except for persulfate concentrations that would coagulate the latex and/or be beyond the solubility of initiator in water at this temperature. It is postulated in the present work that the use of redox initiation may provide a means of extending this data due to the higher capture efficiency of *tert*-butoxy radicals as proposed in this work and their correspondingly high entry rates, to observe for the first time the behaviour predicted by Smith–-Ewart theory (either in its original form or more generalized advances) where, as radical flux is increased, $\bar{n}$ goes from below 0.5, shows a plateau at 0.5, then rises above this plateau.

7.1.1. Calorimetric data

The $\bar{n}$ values determined from calorimetry, when plotted as a function of ρ (Fig. 6) show values similar to, although slightly lower than, those determined by Hawkett [20] in the region where entry rates between the persulfate and redox initiation are expected to overlap, using the diffusion limited entry model developed in the previous sections of this work. These values were plotted against ρ so that a meaningful comparison of the two sets of data could be made as a verification of the entry model, and they qualitatively show the expected $\bar{n} = 0.5$ 'plateau' with only slight changes in $\bar{n}$ across an order of magnitude variation in initiation concentration (and ρ). A substantial increase in $\bar{n}$ was observed for the most concentrated feed corresponding to the highest entry rate, where the particle kinetics have been pushed beyond the regime well described by the zero-one assumption into region where using current termination models it can be shown that the 'instantaneous termination assumption' (the criterion for a system to be zero-one) should break-down.

A calculation of $\bar{n}$ was performed using the method of Maeder and Gilbert [24] as performed previously with values for N_p and r_s of $5.0\times10^{17}\ dm^{-3}$ and 73 nm, respectively. These calculations for values of ρ derived directly from the feed rate are shown in Fig. 15. These calculations show that for all but the most concentrated feed

(where $\bar{n}$ was significantly greater than 0.5 and the zero-one model is not assumed to apply), the experimental value for $\bar{n}$ is within 10% of the calculated value.

Modeling of this data using the full Smith–Ewart treatment, such as that performed in the previous section, was performed to see if the experimentally observed deviation from zero-one kinetics occurs where expected theoretically, and thus providing further support for the proposed entry model. As with the previous analysis, the choice of average termination coefficient can fit a wide range of $\bar{n}$ values whilst using physically reasonable parameters for $\langle k_t \rangle$ (1.0×10^7–$1.0\times10^6\ \mathrm{M^{-1}\,s^{-1}}$). A plot of calculated $\bar{n}$ values using the parameters given in Table 10 is presented in Fig. 16.

As was observed earlier there is theoretical support for an increase in $\bar{n}$ beyond 0.5 for the entry rates postulated here to be found under the highest concentration redox feed. These calculations show that for such entry rates the (chain length independent) Smith–Ewart treatment predicts that the system is no longer in the zero-one limit and indicate that the assumption made in this work of fast initiator radical entry appears to be valid. More sophisticated modeling of such data for high entry rates requires a better treatment of bimolecular termination including chain length dependencies. The data for bimolecular termination available in the literature span an order of magnitude in reasonable values, resulting in a large spread of the possible $\bar{n}$ values and so this has not been pursued further.

7.2. Molecular weight distributions

Another probe for the accuracy of the entry model proposed in this work for the *tert*-butoxy radical species is to determine the molecular weight distributions produced in the systems that were studied calorimetrically above to relate the polymer molecular weight data to entry rates. The SEC data (Fig. 7(a)) correspondingly show a decrease in the molecular weight of the polymer formed during the redox feed as the concentration of initiator is increased. For the most concentrated feed, with an $\bar{n}$ beyond 0.5, a significant shift to lower molecular weights is certainly expected. Rate coefficients can be inferred from the molecular weight distribution in the form of the number distribution $P(M)$, the number of chains with molecular weight M, which is related to the SEC distribution (effectively the SEC signal) $w(\log M)$ by [22,55]:

$$P(M) = \frac{w(\log M)}{M^2} \tag{19}$$

In a zero-one system, $P(M)$ in is given by Eq. (20) [22] which shows that $\bar{M}_n$ should decrease with increasing ρ:

$$P(M) = \exp\left[-\frac{C_p k_{tr,M} + [A]k_{kr,A} + \rho}{k_p C_p}\frac{M}{M_0}\right] \tag{20}$$

A detailed study of the effect upon the molecular weight distributions in redox initiated systems, particularly for large entry rate coefficients, has not been performed in this work but is certainly an area to be considered for future work. However, using the data for feed concentrations of 1×10^{-1}, 1×10^{-2} and 1×10^{-3}% (wt/wt) initiator, a simple normalization based upon the seed polymer distribution and a subsequent subtraction of this seed signal was performed. The MWDs were then plotted as ln $P(M)$ against M, as shown in Fig. 7(b). It has been shown [54,56] that SEC band broadening causes the expected linear form of ln P to become concave-up, and it has also been shown [54,56] that the slope of this concave-up ln P at the molecular weight corresponding to the maximum in $w(\log M)$ is the same as that of the true (i.e. unbroadened) ln $P(M)$: Band-broadening effects cancel at this maximum. This slope, in the absence of chain-transfer agent, should yield an estimate for ρ (using Eq. (20)). The values for ρ determined using this treatment are given in Table 11. This

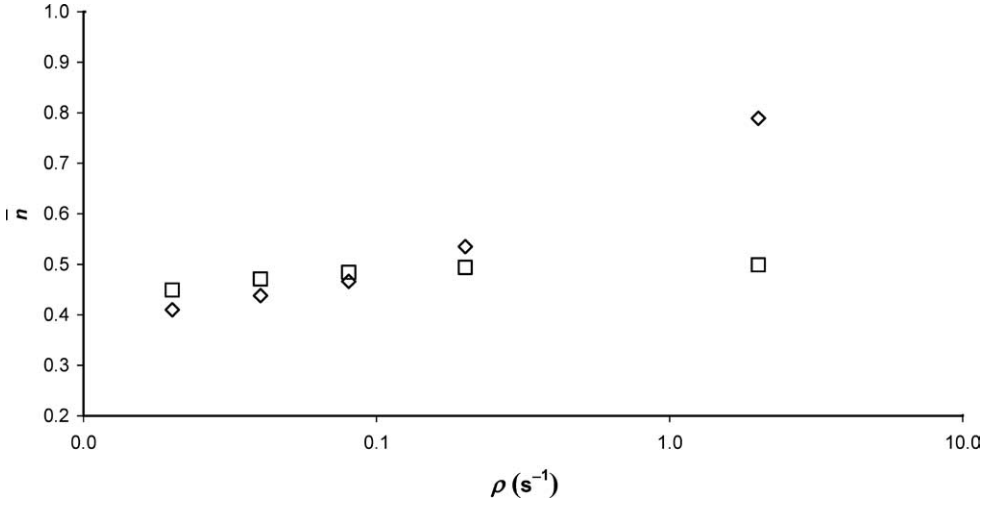

Fig. 15. Comparison of experimental $\bar{n}$ (diamonds) with theoretical zero-one predictions (squares) as a function of ρ for seeded emulsion polymerizations (103 nm diameter seed latex) of styrene using redox initiator.

Table 10
Parameters used in calculation of $\bar{n}$ for comparison with experimental $\bar{n}$ determinations ($r_s = 73.0$ nm and redox initiation using TBHP/Fe/SFS), assuming complete re-entry of exitted radicals

ρ (s^{-1})	2.01, 0.201, 0.0201
k (s^{-1})	5.61×10^{-3}
c (s^{-1})	10.4, 5.19, 1.04

admittedly crude treatment yields values for ρ within an order of magnitude of that predicted by a fast entry (at diffusion-controlled rates) of initiator radicals for the lower two feed concentrations. It also is noted that these values are not directly proportional to the feed rate. This may be due to the unsophisticated treatment of the data or reflect real phenomena. Further study is required to deduce if these values can be trusted, and only then can postulates about modifications to the assumed entry mechanism be made. The agreement is not as satisfactory for the most concentrated feed; however, this system is no longer a simple zero-one system and requires a different form for $P(M)$. This, however, requires a value for the average termination coefficient and so as the previous analysis in this work has shown, assuming a value for this quantity will not be predictive for a single data point. None-the-less this MWD analysis seems to support the kinetic arguments for the diffusion controlled entry of initiator radicals.

8. Concluding remarks

In this study a model describing the entry kinetics of redox initiators has been developed. It has been proposed that initiators can be broadly classed into two categories: Those with hydrophilic radicals and those with hydrophobic radicals. The entry kinetics of hydrophilic species are expected to be well described by the 'Maxwell–Morrison' scheme which results in low initiator efficiencies at high initiator concentrations due to the requirement for aqueous phase propagation. Hydrophobic species, however, have been predicted in this work to enter latex immediately resulting in effectively 100% initiator efficiency under standard conditions. It is possible, therefore, for a redox initiator where the structure of radical species and feed rate are known to predict the steady-state entry rate of radicals into the particle phase.

Table 11
Entry rate coefficients predicted by diffusion-limited entry and those estimated from experimental MWD data for seeded styrene polymerizations using 103 nm seed latex

Feed concentration (% wt/wt)	ρ (s^{-1}, 100% eff.)	ρ (s^{-1}, SEC)
1.0×10^{-1}	2.0	1.5×10^{-1}
1.0×10^{-2}	2.0×10^{-1}	6.6×10^{-2}
1.0×10^{-3}	2.0×10^{-2}	5.6×10^{-2}

To support the proposed model, reaction calorimetry and electrospray mass spectrometry studies of seeded styrene emulsion were performed. Conditions were obtained that enabled reproducible polymerization rates to be observed in a quantitative manner so that kinetic and mechanistic inferences can be made. The observed steady-state kinetics for *tert*-butyl hydroperoxide and sodium formaldehyde sulfoxylate initiated polymerizations indicate that the model indeed well describes the observed entry kinetics. It was also observed however, by additional rate data obtained under non-steady state conditions, that there appears to be a relatively slow rate of radical production for this initiator system; an estimate of the order of magnitude of the rate coefficient for this process was made. Further, it was shown that the two main mechanisms for entry have additional implications for the physical properties of an emulsion system via the formation of in situ surfactant species. This was observed in the polymerization of MMA, in which although the SFS is expected to do little to influence the polymerization kinetics it does impart additional colloidal stability by the production of polymer chains with charged end groups.

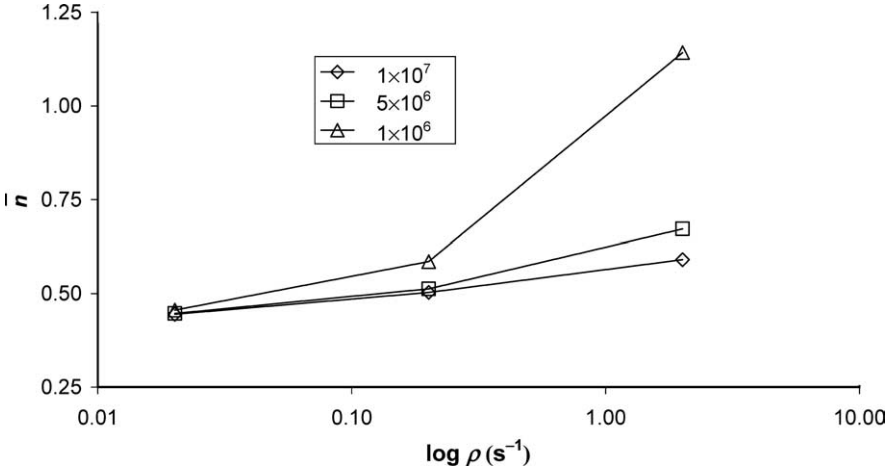

Fig. 16. Predicted $\bar{n}$ as a function of ρ for $\langle k_t \rangle = 1\times10^7$, 5×10^6 and 1×10^6 M^{-1} s^{-1}. Calculated using the method of Ballard [21].

Acknowledgements

The support of BASF AG, and excellent interaction and discussions with Drs Dieter Distler, Jürgen Schmidt-Thuemmes, Brad Morrison, Markus Koppers and Mubarik Chowdry of that company, are gratefully acknowledged. The Key Centre for Polymer Colloids is established and supported under the Australian Research Council's Research Centres program. The RC1 reactor was obtained under an ARC RIEFP grant.

References

[1] Asua JM. J Polym Sci, Part A: Polym Chem 2004;42:1025.
[2] De Bruyn H, Miller CM, Bassett DR, Gilbert RG. Macromolecules 2002;35:8371.
[3] Dong Y, Sundberg DC. Macromolecules 2002;35:8185.
[4] Marestin C, Guyot A, Claverie J. Macromolecules 1998;31:1686.
[5] van Berkel KY, Russell GT, Gilbert RG. Macromolecules 2003;36: 3921.
[6] Maxwell IA, Morrison BR, Napper DH, Gilbert RG. Macromolecules 1991;24:1629.
[7] Gilbert RG. Emulsion polymerization: A mechanistic approach. London: Academic Press; 1995.
[8] De La Rosa LV, Sudol ED, El-Aasser MS, Klein A. J Polym Sci, Part A: Polym Chem 1996;34:461.
[9] De La Rosa LV, Sudol ED, El-Aasser MS, Klein A. J Polym Sci, Part A: Polym Chem 1999;37:4073.
[10] De La Rosa LV, Sudol ED, El-Aasser MS, Klein A. J Polym Sci, Part A: Polym Chem 1999;37:4066.
[11] De La Rosa LV, Sudol ED, El-Aasser MS, Klein A. J Polym Sci, Part A: Polym Chem 1999;37:4054.
[12] Ozdeger E, Sudol ED, El-Aasser MS, Klein A. J Polym Sci, Part A: Polym Chem 1997;35:3837.
[13] Ozdeger E, Sudol ED, El-Aasser MS, Klein A. J Polym Sci, Part A: Polym Chem Ed 1997;35:3813.
[14] Ozdeger E, Sudol ED, El-Aasser MS, Klein A. J Polym Sci, Part A: Polym Chem 1997;35:3827.
[15] Blythe PJ, Klein A, Phillips JA, Sudol ED, El-Aasser MS. J Polym Sci, Part A: Polym Chem 1999;37:4449.
[16] Lamb DJ, Fellows CM, Morrison BR, Gilbert RG. Polymer 2005;46: 285.
[17] Lansdowne SW, Gilbert RG, Napper DH, Sangster DF. J Chem Soc Faraday Trans 1 1980;76:1344.
[18] Scheren PAGM, Russell GT, Sangster DF, Gilbert RG, German AL. Macromolecules 1995;28:3637.
[19] Kangwansupamonkon W, Fellows CM, Lamb DJ, Gilbert RG, Kiatkamjornwong S. Polymer 2004;45:5775.
[20] Hawkett BS, Napper DH, Gilbert RG. J Chem Soc Faraday Trans 1 1980;76:1323.
[21] Ballard MJ, Gilbert RG, Napper DH. J Polym Sci, Polym Lett Ed 1981;19:533.
[22] Clay PA, Gilbert RG. Macromolecules 1995;28:552.
[23] Prescott SW, Ballard MJ, Gilbert RG. J Polym Sci, A Polym Chem Ed 2005;43:1076.
[24] Maeder S, Gilbert RG. Macromolecules 1998;31:4410.
[25] Casey BS, Morrison BR, Maxwell IA, Gilbert RG, Napper DH. J Polym Sci, Part A: Polym Chem 1994;32:605.
[26] Gilbert RG, Napper DH. J Macromol Sci Rev Macromol Chem Phys C 1983;23:127.
[27] De Buruaga IS, Arotcarena M, Armitage PD, Gugliotta MM, Leiza J R, Asua JM. Chem Eng Sci 1996;51:2781.
[28] Buback M, Gilbert RG, Hutchinson RA, Klumperman B, Kuchta F-D, Manders BG, et al. Macromol Chem Phys 1995;196:3267.
[29] Prescott SW. Macromolecules 2003;36:9608.
[30] Lane WH. Ind Eng Chem 1946;18:295.
[31] van Doremaele GHJ, Geerts FHJM, Schoonbrood HAS, Kurja J, German AL. Polymer 1992;33:1914.
[32] Eichenauer H. Germany Patent DE 10060410; 2002.
[33] Oxenrider BC, Mares F, Yang MS. US Patent US 5453477; 1995.
[34] Denicola AJJ, Syed A. US Patent US 5817707; 1997.
[35] Lorah DP, Slone RV. US Patent US 2002065381; 2002.
[36] Baxter SM, Clark PA. US Patent US 2002099156; 2002.
[37] Tanimoto S, Inomata N, Murakami T. Japan Patent JP 2003277411; 2003.
[38] da Cunha L, Ilundain P, Salazar R, Alvarez D, Barandiaran MJ, Asua J M. Polymer 2001;42:391.
[39] Christie DI, Gilbert RG, Congalidis JP, Richards JR, McMinn JH. Macromolecules 2001;34:5158.
[40] Kast H, Funke W. Makromol Chem 1981;182:1553.
[41] Kast H, Funke W. Makromol Chem 1981;182:1567.
[42] Said ZFM, Hassan SA, Dunn AS. In: Bassett DR, Hamielec AC, editors. ACS symposium series: Emulsion polymers and emulsion polymerization. Washington, DC: American Chemical Society; 1981. p. 471.
[43] De Bruyn H, Hawkett BS, Gilbert RG. Polymer 2000;41:8633.
[44] Ebdon JR, Huckerby TN, Hunter TC. Polymer 1994;35:250.
[45] Makarov SV. Russian Chem Rev 2001;70:885.
[46] Prieto F, Coles BA, Compton RG. J Phys Chem B 1998;102:7442.
[47] Russell GT, Napper DH, Gilbert RG. Macromolecules 1988;21:2141.
[48] Russell GT, Gilbert RG, Napper DH. Macromolecules 1992;25:2459.
[49] Morrison BR, Casey BS, Lacík I, Leslie GL, Sangster DF, Gilbert RG, et al. J Polym Sci, Part A: Polym Chem 1994;32:631.
[50] Lichti G, Gilbert RG, Napper DH. J Polym Sci A 1980;18:1297.
[51] Clay PA, Christie DI, Gilbert RG. In: Matyjaszewski K, editor. Advances in free-radical polymerization. American Chemical Society: Washington, DC; 1998. p. 104.
[52] Walling C. Acc Chem Res 1975;8:125.
[53] Orr RJ, Williams HL. J Org Chem 1953;57:925.
[54] van Berkel KY, Russell GT, Gilbert RG. Macromolecules 2005;38: 3214.
[55] Shortt DW. J Liq Chromatogr 1993;16:3371.
[56] Castro JV, van Berkel KY, Russell GT, Gilbert RG. Aust J Chem 2005;58:178.